

We are IntechOpen, the world's leading publisher of Open Access books Built by scientists, for scientists

4,800

Open access books available

122,000

International authors and editors

135M

Downloads

Our authors are among the

154

Countries delivered to

TOP 1%

most cited scientists

12.2%

Contributors from top 500 universities



WEB OF SCIENCE™

Selection of our books indexed in the Book Citation Index
in Web of Science™ Core Collection (BKCI)

Interested in publishing with us?
Contact book.department@intechopen.com

Numbers displayed above are based on latest data collected.
For more information visit www.intechopen.com



Simulation of Rigid-Limit and Slow-Motion EPR Spectra for Extraction of Quantitative Dynamic and Orientational Information

Andrey Kh. Vorobiev and Natalia A. Chumakova

Additional information is available at the end of the chapter

<http://dx.doi.org/10.5772/74052>

1. Introduction

The present chapter is devoted to methods of extraction of quantitative data from slow-motion EPR spectra of nitroxides in viscous and rigid media. Slow-motion spectra correspond to the range of rotation relaxation times in which the EPR spectra cannot be reduced to superposition of the Lorentzian lines, which is typical of the range of fast rotation. In the case of the X-band EPR spectra of nitroxides, this range lies approximately from 10^{-6} to 10^{-9} s. In the limit of slow motions the movements of the probe do not influence the EPR spectrum shape (rigid-limit conditions). The aim of the present chapter is to describe the methods of yielding quantitative data on molecular mobility and orientation alignment. Such data can be obtained most reliably by means of numerical simulation of the spectra. In the appendix of this chapter, we describe the homemade software used for spectra simulation.

The methods of extraction of quantitative data on molecular mobility from EPR spectra have been developed rather intensively during the last decades. In the case of fast rotation (characteristic time shorter than approximately 10^{-9} s), the simple measurements of line widths and intensities of spectral components are enough to estimate the isotropic rotation correlation time. The corresponding procedures and formulas can be found elsewhere [1-3]. When more exact data are desirable and in the case of anisotropic rotational mobility, the well-known method developed by Freed and collaborators for numerical simulation of the spectra can be used [4, 5]. Examples of applications of this technique to different systems can be found in works [6-11].

In the present chapter, we focus the reader's attention on obtaining quantitative data when the conventional methods produce incorrect or unreliable results. Section II describes the method of determining the translational diffusion coefficient. The technique is simple and

does not require spectra simulation. It was suggested in [12] about 20 years ago but has not found wide application. We illustrate this technique on samples of ordinary solvents and ionic liquids. The methods of spectra simulation are considered in section III. First, in the rigid-limit spectra of the isotropic samples, we showed the possibility to achieve agreement between experimental and calculated spectra within errors of spectrum recording. The magnetic and line width characteristics of the nitroxide probe are determined in the course of this simulation. The obtained values are necessary for the analysis of spectra recorded in more complicated conditions. The spectra simulation and determination of the rotational characteristics of the probes in polymer matrices are presented as examples. The quantitative description of EPR spectra in a wide temperature range up to the glass transition point was found to require consideration of quasi-libration movements. Section IV deals with the study of orientation alignment of paramagnetic probes. The section describes the orientation distribution functions that can be determined by simulation of spectrum angular dependencies. Liquid crystalline, polymeric, and low-molecular glassy systems are considered. The model-free method of characterizing orientation distribution function is compared with the mean-force approach realized in the known software [4, 5]. The advantages and drawbacks of both approaches are discussed.

2. Determination of the translation diffusion coefficients of the paramagnetic molecules from the analysis of temperature dependence of EPR spectra concentration broadening

It is well known that the spin probe technique can be used to measure molecular rotational mobility, as the rotational movements are reflected in the width and shape of EPR spectrum lines [1-5]. On the contrary, translational molecular mobility of paramagnetic molecules is studied by EPR technique very rarely. Meanwhile, it is known that translation of radicals influences EPR spectrum. There are two underlying mechanisms of this influence: dipole-dipole interaction and spin (Heisenberg) exchange. Both of these mechanisms lead to broadening of the spectral lines. At low temperatures, when translational mobility is substantially hindered, the main cause of spectral line broadening is the dipole-dipole interaction of paramagnetic molecules. At high temperatures, the intensive translational movements average the dipole-dipole interaction of radicals while increasing spin exchange. It is obvious that there exists a temperature region where the contributions of dipole-dipole and exchange interactions to line broadening are comparable. A theoretic research [13] showed earnestly the difficulty of a direct analysis of the EPR spectra with the purpose of determining the translational diffusion coefficients. Nevertheless, the translational diffusion coefficients may be estimated by an analysis of the broadening of EPR spectra. For this purpose, the method described in [12, 14-16] can be used. This method allows estimating contributions of dipole-dipole and exchange interactions to the line width by means of analyzing the temperature dependence of the concentration broadening. The concentration broadening can be represented as follows:

$$\delta H = [A \exp(-E_{tr}^a / kT) + B \exp(E_{tr}^a / kT)] \delta c, \quad (1)$$

where δH is the line broadening, E_{tr}^a is the effective activation energy of translational movement, and δc is the difference in concentrations of two radical solutions. The first summand in Eq. (1) describes the effect of the exchange broadening, and the second term describes the effect of the dipole-dipole interaction.

The widths of the spectral lines are determined as the distances between the points of the maximal slope of the absorption lines (peak-to-peak distances of the first derivatives of the absorption lines). In the paper [12], the application of this method in determining the translational diffusion coefficients of the various spin probes in liquid crystal matrices was demonstrated. In the joint work with our colleagues from the University of Graz (Austria), we showed the possibility of using the method to investigate the translation of radicals in standard low-molecular-weight solvents and room-temperature ionic liquids [17].

In Figure 1, one can see the EPR spectra recorded for two different concentrations of radical TEMPOL-d17 in glycerol at various temperatures. It is obvious that the spectra of the solution with a larger concentration are broadened noticeably in comparison with the spectra of the less concentrated solution. Because the rotational mobility of the radicals does not depend on concentration, the difference observed was therefore caused by the dipole-

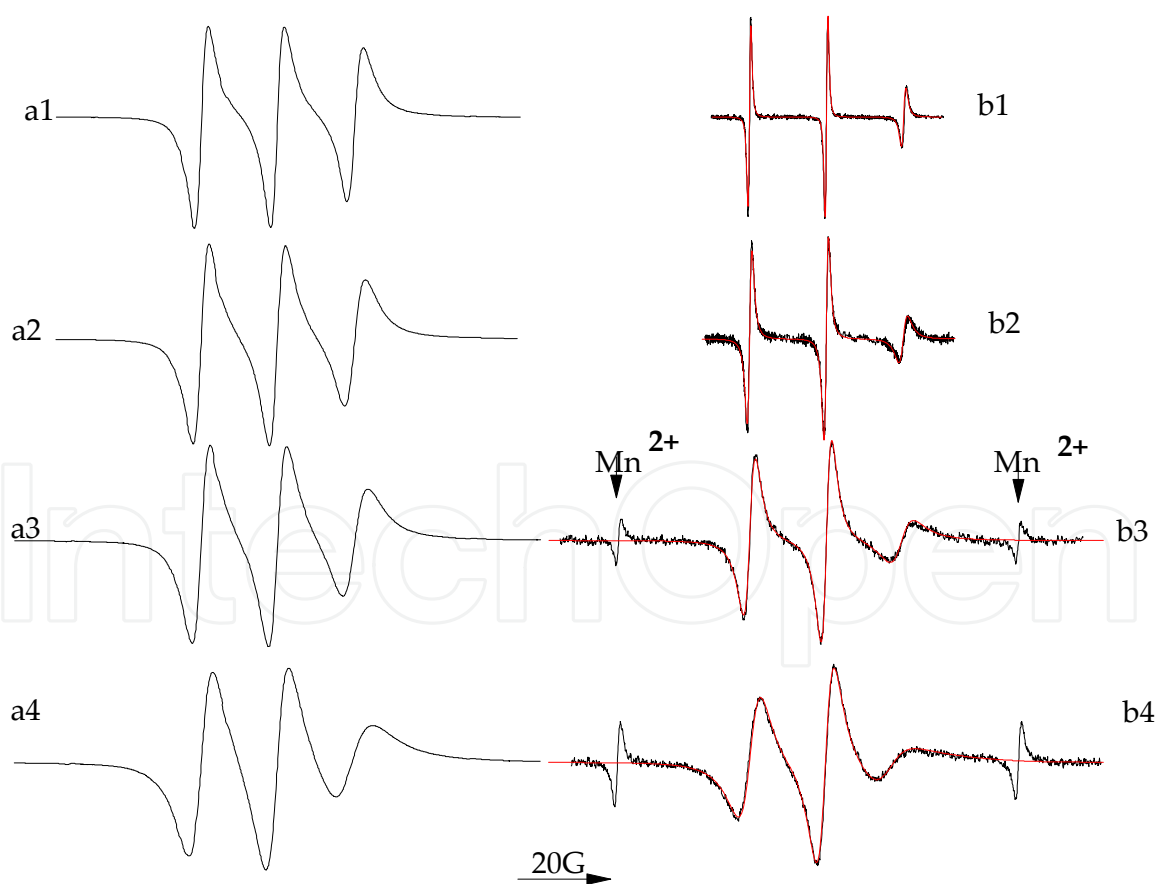


Figure 1. The EPR spectra of TEMPOL-d17 in glycerol: (a) 7.1×10^{-2} mol/L and (b) 3.0×10^{-3} mol/L, recorded at temperatures 333K (a1, b1), 318K (a2, b2), 303K (a3, b3), and 295K (a4, b4). The red lines are the results of the simulation of the spectra according to the method described in [4,5].

dipole and exchange interactions of the paramagnetic molecules. The result of the computer simulation of the spectra for the solution with low concentration of the radicals is also presented in Figure 1. The simulation was performed according to [5] and was used to determine the rotation diffusion coefficients of TEMPOL-d17 in glycerol at different temperatures and estimation of the effective activation energy of the rotational movements.

Figure 2(a) presents the temperature dependence of the line broadening δH normalized on the difference of concentrations δc for radical TEMPOL-d17 in glycerol and the result of fitting the experimental data according to Eq. (1). The modeling was performed by the least squares method, with simultaneous variation of three parameters: A , B , and $E^{a_{tr}}$. In this figure, one can also see the calculated contributions of the exchange and dipole-dipole broadening. Obviously, at temperatures 320–330K, the line broadening is caused mainly by the dipole-dipole interactions of the radicals, whereas at 360–370K, the lines are broadened basically by spin exchange. At the intermediate temperature range 340–360K, the contributions of dipole-dipole and exchange broadening are comparable. The effective activation energies of the rotational and translational movements of the radicals TEMPOL-d17 in glycerol are presented in Table 1.

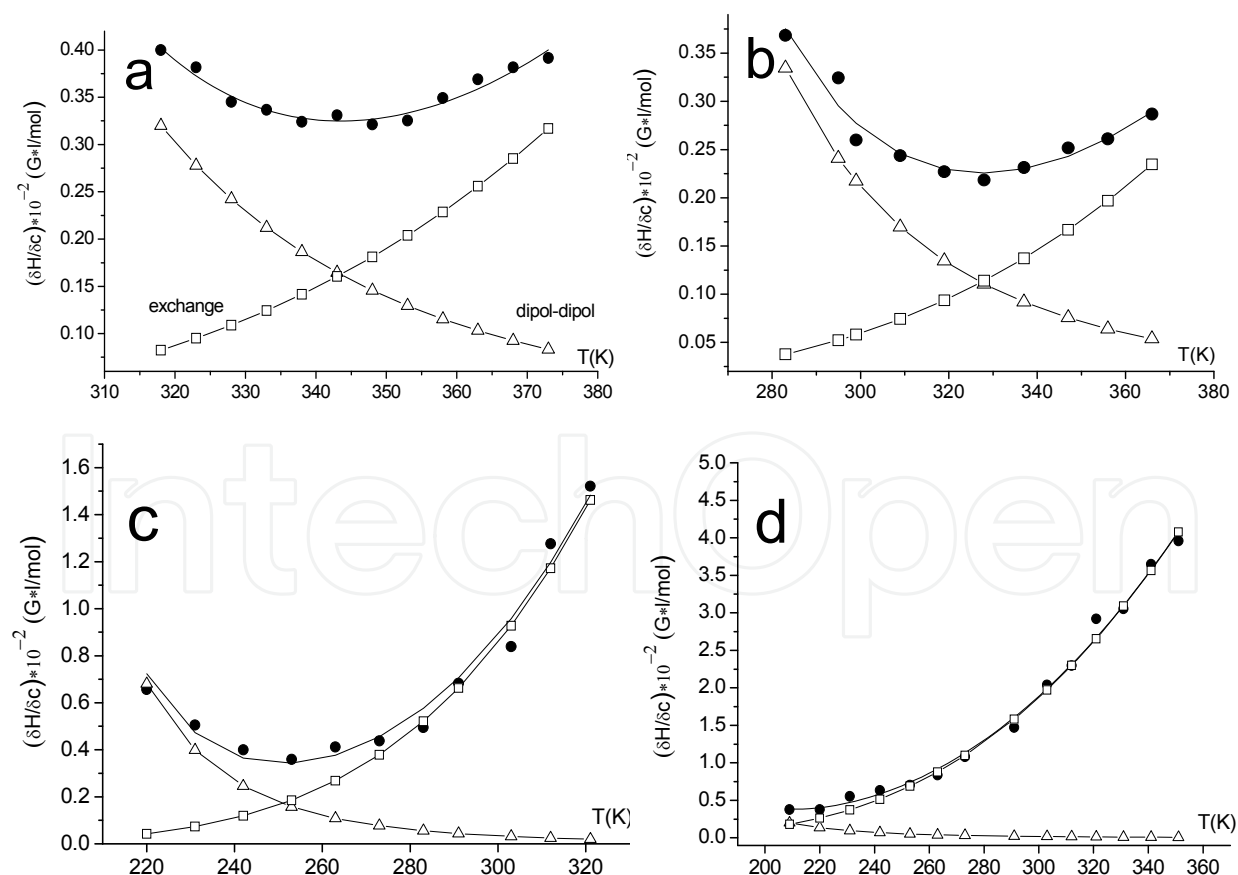


Figure 2. $\delta H/\delta c$ as a function of temperature for TEMPOL-d17 in glycerol (a), TEMPOL in omimBF4 (b), 1-propanol (c), and cumene (d); experimental broadening (solid circles); contribution of spin exchange (open squares); and contribution of dipole-dipole interaction (open triangles).

Matrix	$E_{\text{rot}}^{\text{a}}/\text{kJ}\cdot\text{mol}^{-1}$	$E_{\text{tr}}^{\text{a}}/\text{kJ}\cdot\text{mol}^{-1}$
emimBF ₄	26.8 ± 0.6 (280–360K)	8.4 ± 1.1 (295–380K)
bmimBF ₄	37.5 ± 0.8 (260–350K)	15.8 ± 1.1 (295–380K)
omimBF ₄	36.1 ± 0.4 (280–400K)	19.0 ± 1.2 (295–380K)
omimPF ₆	47.6 ± 1.3 (280–370K)	15.3 ± 1.0 (295–380K)
omimCl	38.7 ± 1.4 (290–360K)	20.4 ± 0.5 (295–380K)
glycerol*	49.4 ± 0.8 (295–345K)	24.1 ± 1.0 (320–380K)
cumene	18.4 ± 0.9 (200–290K)	13.4 ± 0.6 (210–360K)
<i>n</i> -propanol	18.0 ± 0.6 (200–290K)	20.5 ± 1.4 (220–320K)

* Radical TEMPOL-d17

Table 1. The effective activation energies of the rotational and translational moves of the radicals TEMPOL in different matrices

Consideration of spin-exchange contribution to spectral broadening makes it possible to calculate the spin-exchange constant as follows [18]:

$$k_{\text{exch}} = [1.52 \cdot 10^7 (g/2)(2/3)(\delta H)_{\text{exch}}] / \delta c, \quad (2)$$

where g is the average value of the g -factor of the radical, δH_{exch} is the contribution of spin exchange to the broadening of the spectra.

On the basis of the spin-exchange constant, it is easy to calculate the translation diffusion coefficient [18]:

$$D_{\text{tr}} = k_{\text{exch}} / 16 f \pi r, \quad (3)$$

where f is the steric factor reflecting different probability of spin exchange upon collisions with different mutual orientations of the radicals (for TEMPOL, $f = 0.8$ [19]) and r is the radius of the paramagnetic molecule.

The translational diffusion coefficients of the TEMPOL-d17 in glycerol, calculated at some temperatures, are presented in Table 2.

In Figure 2(b–d), the examples presented illustrate the application of the method [12] in determining the translational diffusion coefficients of the undeuterated probe TEMPOL in the ionic liquid omimBF₄ and standard molecular solvents *n*-propanol and cumene. The

high temperature spectra of the diluted solutions of undeuterated TEMPOL demonstrate the additional hyperfine structure on protons. In these cases, we measured the width of the envelope of the spectral line. It can be seen that such method does not lead to distortion of the temperature dependence of the spectral line broadening. Indeed, intensive spin exchange at high temperatures and large concentration leads to substantial spectral line broadening. As a result, subtraction of a small value measured with some error from a big value measured exactly does not lead to a significant error in the result. The values of the effective activation energies for translation and rotation of the radical TEMPOL in different matrices are presented in Table 1.

In Figure 2(c, d), one can see the temperature dependence of the EPR spectra broadening for TEMPOL in the low-viscous solvents *n*-propanol and cumene. It is seen that in these cases, the temperature range in which the dipole-dipole broadening can be observed is confined significantly. At lower temperatures, the rotational mobility of the probe is so small that measurement of the spectral line widths becomes impossible. In the case of *n*-propanol, the parabolic dependence (1) has feebly marked the left dipole-dipole branch (viscosity at room temperature, $\eta_{295} = 1.8$ sP). In the case of cumene ($\eta_{295} = 1.0$ sP), we can observe practically only the exchange branch of the concentration broadening. However, even in this case, it is possible to distinguish the significantly different contributions of dipole-dipole interaction and spin exchange to broadening of the spectral lines by means of the method [12].

	220K	240K	260K	280K	295K	300K	320K	340K	360K	380K
emimBF ₄	–	–	–	–	1.9	2.0	2.5	3.0	3.6	4.2
bmimBF ₄	–	–	–	–	1.1 ± 0.4 0.8 ± 0.3* 0.9 ± 0.3**	1.3	1.9	2.7	3.7	4.8
omimBF ₄	–	–	–	–	0.6	0.7	1.0	1.6	2.4	3.3
omimPF ₆	–	–	–	–	0.9	1.0	1.5	2.1	2.8	3.7
omimCl	–	–	–	–	0.3	0.4	0.6	0.9	1.4	1.9
glycerol***	–	–	–	–	–	–	1.0	1.7	2.7	4.1
cumene	3.0	5.5	9.2	14.3	19.2	21.0	29.4	39.6	51.5	–
<i>n</i> -propanol	0.5	1.2	2.7	5.4	8.4	9.6	16.1	–	–	–

*The data were obtained by means of cyclic voltammetry

**The data were obtained by means of chronoammetry

***Radical TEMPOL-d17

Table 2. The translation diffusion coefficients ($D_{tr} \cdot 10^7$) of the radical TEMPOL at various temperatures

Recently it was supposed [20-22] that paramagnetic molecules in the solvent cage repeatedly collide and exchange their spin states. In such case the spin exchange does not reflect adequately the rate of translational diffusion of molecules in the medium. To check the correctness of the obtained data we compared the value of translation diffusion coefficient

of TEMPOL in ionic liquid bmimBF₄ with the values measured for the same system by two independent electrochemical methods - cyclic voltammetry and chrono-ammetry [23]. The results of all types of measurements are in agreement within experimental errors (Table 2).

From Table 2, it can be seen that in cases of viscous solvents, the effective values of activation energy for rotational mobility exceed noticeably the effective values of activation energy for translational movements. The reason of this phenomenon is not clear at the present time. Perhaps it is a result of microstructure of viscous solvents, such as glycerol, and all ionic liquids.

We hope that the method of determining the translation diffusion coefficients of paramagnetic molecules [12], which possibly does not possess high accuracy but is very simple to use and does not demand computer simulation of the spectra, will be widely applicable.

3. Simulation of EPR spectra in glassy polymer matrices: Rigid-limit and quasi-libration model

The example presented earlier demonstrates that simple semi-empirical treatment of EPR spectra can provide useful information concerning the dynamic properties of condensed media. Numerous examples prove, however, that numerical modeling of experimental EPR spectra leads to more unambiguous and reliable results. Therefore, methods of simulation of EPR spectra are the main subject of the present chapter. In earlier works, simulation of spectra was based on the trial-and-error method. The researcher chose the parameters of the EPR spectrum, taking into account theoretical consideration or analogy with known results, and calculated the spectrum. The quality of the calculated spectrum was determined by visual comparison with the experimental one. The parameter values were then adjusted to improve the agreement with the experiment. This approach is often used up to the present. However, most investigators currently use the numerical fitting of experimental spectra with variation of parameters. In this technique, the desirable values are determined in the course minimizing the discrepancy between the calculated and experimental spectra by means of nonlinear least-squares fitting procedures. The higher objectivity of this technique and the possibility of determining errors make this approach preferential. The different fitting algorithms are compared in [24]. The minimizing program NL2SOL [25] was used in the present work.

The shape of the EPR spectrum can be calculated using a different software, for example, EasySpin (<http://www.easyspin.org/>) and SimFonia (<http://www.bruker-biospin.com/xsophe.html>). We used the homemade software described in the appendix of the present chapter. Unweighted differences between the experimental and simulated spectra, which are calculated in each point of the spectrum, are used as minimized residuals r_i . The resulting discrepancy is calculated as follows:

$$D = \frac{1}{2} \sum_i \frac{r_i^2}{n}, \quad (4)$$

where n is the number of calculated points in the spectrum.

Since the simulation of the ESR spectra via the determination of required parameters is an inverse problem, some restrictions should be imposed on the simulation results to avoid ambiguity. We consider the description of the ESR spectra as satisfactory when the following requirements are met:

1. The discrepancies between the simulated and experimental spectra should be within the experimental errors.
2. The resulting optimal set of parameters should be stable. The simulation procedure should converge to the same optimal set of parameters, independent of the choice of initial parameter values within physically reasonable limits.
3. The resulting values of the magnetic and dynamic parameters and the values of the parameters of individual line width should be physically meaningful.

Numerical simulation of the EPR spectra is used mainly with two aims: to determine the structural, dynamic, or chemical properties of the paramagnetic particle studied and to estimate the characteristics of the medium under consideration (spin probe technique). The determination of magnetic parameters of paramagnetic species is a necessary step in the study in both cases. The determination of magnetic parameters is more reliable when complicated factors, such as molecular mobility, intramolecular transitions, dipole-dipole broadening, and orientation alignment, are absent. Hence, the measurements of magnetic parameters are often performed using diluted glassy solutions at low temperatures, when molecular mobility is frozen (rigid-limit conditions). The simulation of rigid-limit spectra is considered in the next section in more detail. This problem will be used to illustrate the strategy of fitting procedure and to discuss the possible troubles and errors. The structures of the nitroxide probes used are shown in Figure 3.

3.1. Quality of the experimental spectra

The requirement of coincidence of experimental and calculated spectra within experimental errors impose the following additional conditions on the procedure of spectra recording:

1. Modulation amplitudes should be less than the characteristic features of the spectrum shape. The most reliable way to check the fulfillment of this condition is recording the spectrum with different modulation amplitudes and comparing the spectra obtained.
2. The microwave power should not induce saturation. To check this condition, the recording spectrum at a different microwave power is necessary. The signal amplitude then is plotted versus the square root of power. The appropriate power is chosen within the linear part of this dependency. This check is particularly important when low-temperature spectra disposed to saturation are recorded.
3. The field range for the recorded spectra should contain sufficiently long left and right “tails,” where the signal is negligibly small. The baseline should be carefully subtracted from the spectrum using the tail fragments.
4. The recorded spectrum should be checked for the absence of the “fast passage” effect [26], which is seen more often in solids at low temperatures. This effect leads to superposition of the integral signal of dispersion and the first derivative EPR lines. To check the absence of this effect, the calculation of the first moment should be used. If the

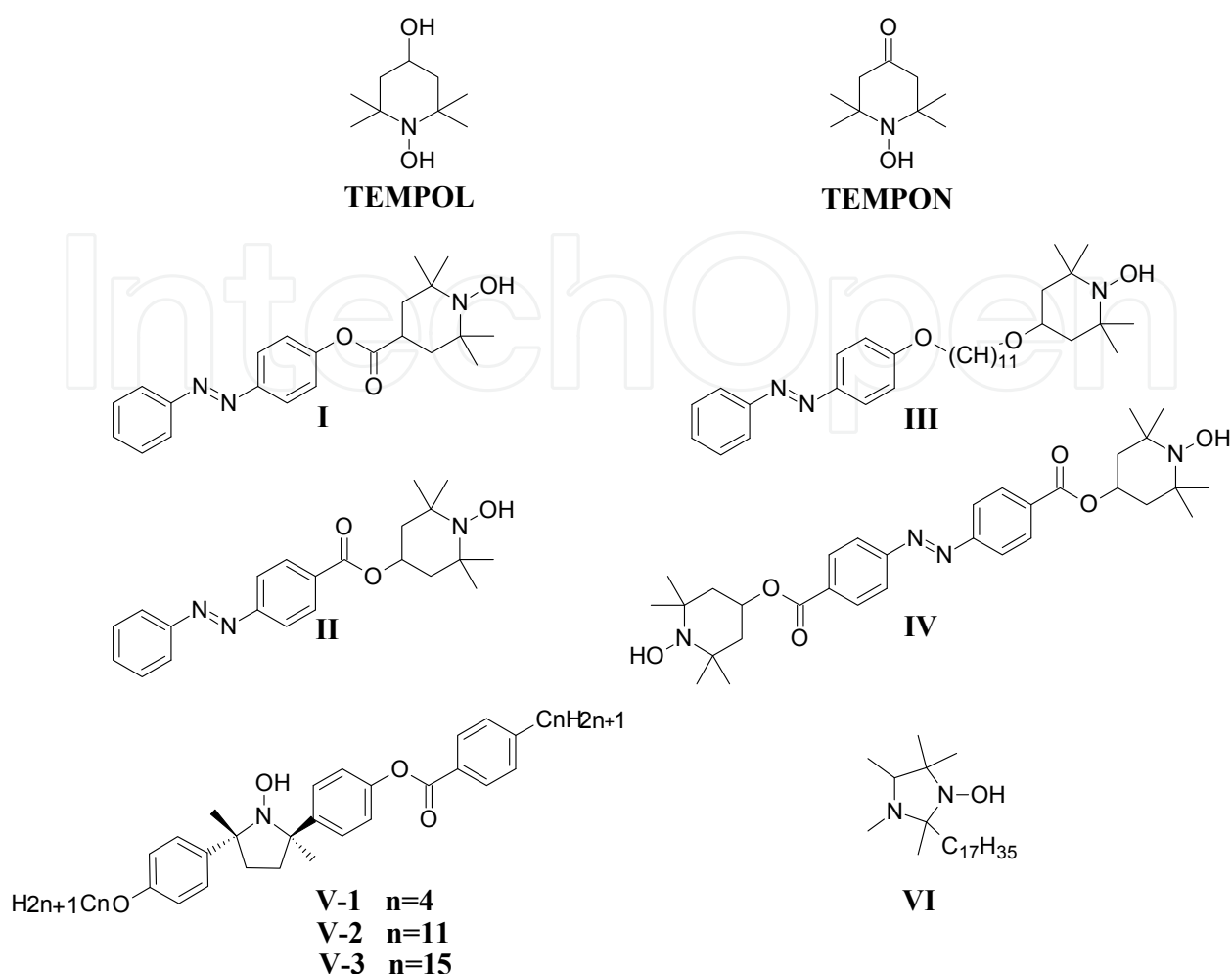


Figure 3. The structures of the nitroxide probes used.

center of the spectrum is taken as zero point, the value of the first moment calculated for the left part of spectrum should be equal to the value of the first moment calculated for the right part. This calculation is useful for controlling baseline subtraction as well. Our practice showed that the spectra with differences of less than 10% between the values of the left and right first moments are acceptable for simulation.

Before the simulation, the experimental spectra are normalized so that the spectrum area is equal to unity. In this case, the final discrepancies between the experimental and calculated spectra for the different experiments can be compared.

For these checks, subtractions, and other manipulations with the experimental spectra, the homemade program *esrD* is used in our laboratory. The short description of the program is presented in the appendix of this chapter.

3.2. Simulation of rigid-limit EPR spectra

The shape of the EPR spectrum of the disordered sample in rigid-limit conditions is described by the following expression:

$$F(H) = \frac{1}{4\pi} \int_0^{2\pi} d\varphi \int_0^{\pi} f(H, g, A, \theta, \varphi) \sin \theta d\theta, \quad (5)$$

where angles θ , φ define the magnetic field direction in the frame of paramagnetic species, $f(H, g, A, \theta, \varphi)$ is the shape of the individual resonance line, the position of the resonance line is defined by the g value $g(\theta, \varphi)$ and by the hyperfine interaction constant $A(\theta, \varphi)$, and the shape of the resonance line is described by the width and type of function (Gaussian, Lorentzian, or mixed function).

Sufficient description of the magnetic properties of the paramagnetic probe consists in determining three g -tensor components, three components of hfi tensor for each magnetic nucleus, three Euler angles connecting each hfi frame with g -tensor frame, and the characteristics of an individual resonance line. Determination of the magnetic parameters of a paramagnetic particle in case of several nuclei with noticeable hyperfine interaction is a rather complicated problem that remains unsolved in full measure up to the present. Fortunately, only the hfi on a nitrogen nucleus is usually apparent in the EPR spectra of nitroxides. The hyperfine interaction with the protons in nitroxides is weaker by two orders of magnitude and thus can be neglected. For further simplification of the EPR spectrum, the isotope-substituted compounds are used. In this case, the hydrogen atoms in the probe molecule are replaced by deuterium and/or ^{14}N nucleus (spin 1) is replaced by ^{15}N (spin 1/2).

3.2.1. Shape and width of the individual line

The condition of coincidence of the calculated and experimental spectra within the errors of the experiment requires application of the most comprehensive function of line shape. It is the convolution of Gaussian and Lorentzian functions (Voigt profile). Such convolution is calculated mostly using fast Fourier transformation. We have found, however, that this procedure is insufficiently stable in the course of line width variation. Using equation (6)[27],

$$\int_{-\infty}^{+\infty} \frac{t \cdot \exp(-y^2) dy}{(x-y)^2 + t^2} = \pi \cdot \text{Re} \omega(x + it), \quad (6)$$

where $\omega(z) = \exp(-z^2) \cdot \text{erfc}(-iz)$ and $\text{erfc}(x) = \frac{2}{\sqrt{\pi}} \int_x^{\infty} e^{-t^2} dt$ are the additional probability integral, the following explicit expression for the first derivative of the absorption line can be obtained:

$$F'(H) = \frac{4}{h_G^2 \sqrt{\pi}} \text{Re}[z \cdot \exp(-z^2) \cdot \text{erfc}(-iz)] \quad (7)$$

$$z = \frac{(H - H_0)\sqrt{2}}{h_G} + i\sqrt{\frac{3}{2}} \frac{h_L}{h_G}$$

where $H-H_0$ is distance from the center of the line, h_G is the Gaussian line width, and h_L is the Lorentzian line width.

Expression (7) should be used in the course of fitting despite the fact that numerical procedure becomes sufficiently slower.

It is known also that the line width of the EPR spectrum depends on the orientation of the paramagnetic particle relative to the magnetic field of the spectrometer. It means that both line width values, $h_G = h_G(\theta, \varphi)$ and $h_L = h_L(\theta, \varphi)$, are orientation dependent. To take into account this dependence, we describe the Gaussian and Lorentzian line widths as second-rank tensors, which can be tilted relative to g-tensor axes.

3.2.2. Number of fitting parameters and the uniqueness of their determination

The fitting parameters that are used in the course of the simulation of rigid-limit EPR spectrum are listed in Table 3. It is seen from Table 3 that the number of adjustable parameters for the rigid-limit simulation in the general case can reach 23. We do not know the examples of determination of all these values from the simulation of the EPR spectra. As a rule, some of the indicated parameters do not influence significantly the agreement between the calculated and experimental spectra. The attempt to determine such values by the fitting procedure leads to false or singular convergence in the course of minimization. In that case, spectrum fitting should be repeated after elimination of the indefinable values from the set of varied parameters. Other varied values can come to zero in the course of minimization. It means that this parameter is well defined by the EPR spectrum, but in the course of minimization, this parameter also can be removed from the set of variables.

The ambiguity of the values determined and several minima with the comparable description of the experimental spectrum can be observed when two or more parameters equally influence the spectrum. Such improper parameters can be revealed by an analysis of covariance matrix calculated in the final point of minimization. The values that demonstrate the covariance coefficients more than 0.7–0.8 are not sufficiently independent and possibly cannot be determined simultaneously.

In the course of simulation of the EPR spectra of nitroxides, such troubles appear first at the determination of the Euler angles that describe the relative orientation of different molecular frames related with the tensors shown in Table 3. In particular, the tilt of the axes of the Gaussian and Lorentzian line width tensors are determined from the rigid-limit EPR spectra exceptionally rarely. Commonly, it is enough to assume that the principal frames of these tensors coincide with the g-tensor frame. The determination of the orientation of the hfi-tensor frame relative to the g-tensor frame is also a rare case, as the structure of nitroxides usually dictates almost complete coincidence of these frames.

Sometimes the interdependence is observed between the values of the hfi components and the corresponding components of the Gaussian and Lorentzian line width, namely, between values A_x , h_{Lx} , and h_{Gx} and between values A_y , h_{Ly} and h_{Gy} . This interdependence is a result of insufficient resolution of the spectra when the value of the line width is comparable

Fitting parameters	Description	Number of parameters and their determinability in the course of simulation of the nitroxide EPR spectrum
I	Spectrum intensity	1*
Field shift	Microwave frequency or $\langle g \rangle$ value or field shift is varied to adjust the field position of the calculated and experimental spectra	1*
g_x, g_y, g_z	Principal values of the electronic g-tensor Only two values are varied simultaneously; the third one is defined by isotropic value, if it is known: $\langle g \rangle = (g_x + g_y + g_z) / 3$	2, 3*
A_x, A_y, A_z	Principal values of the nuclear hfi tensor Only two value are varied simultaneously; the third one is defined by isotropic value, if it is known: $\langle A \rangle = (A_x + A_y + A_z) / 3$	2, 3**
$\Omega(A \rightarrow g)$	Euler angles connecting the own frame of the hfi tensor with the own frame of the g-tensor	3**
h_{Lx}, h_{Ly}, h_{Lz}	Principal values of the orientation-dependent Lorentzian tensor of line width	3*
$\Omega(h_L \rightarrow g)$	Euler angles connecting the own frame of the h_L tensor with the own frame of the g-tensor	3**
h_{Gx}, h_{Gy}, h_{Gz}	Principal values of the orientation-dependent Gaussian tensor of line width	3*
$\Omega(h_G \rightarrow g)$	Euler angles connecting the own frame of the h_G tensor with the own frame of the g-tensor	3**

*Parameters are easily determined

**Some troubles are observed in the course of parameter determination

Table 3. Fitting parameters

with the values of hyperfine splitting. This interdependence is vanished when the deuterated probes are used. To obtain more resolved spectra and more precise determination of A_x and A_y values, the spectra recording at higher temperatures is often used. For example, the magnetic parameters for a number of nitroxides presented in [28] were determined from the spectra recorded at a temperature below glass transition point but higher than 77K. It should be taken into account that narrowing of the spectrum at higher temperatures indicates appearance of some intramolecular or intermolecular mobility. Thus, the obtained values can be slightly averaged by molecular movements. Partial averaging of magnetic parameters by molecular mobility in low-temperature glassy matrices will be considered in detail in section III.3.

The number of varied parameters diminishes when tensors taken into account have uniaxial or isotropic symmetry. The number of parameters that can be varied simultaneously commonly does not exceed 10–15.

3.2.3. Examples of rigid-limit EPR spectra simulations

The examples of X-band EPR spectra described by the fitting procedure are presented in Figure 4.

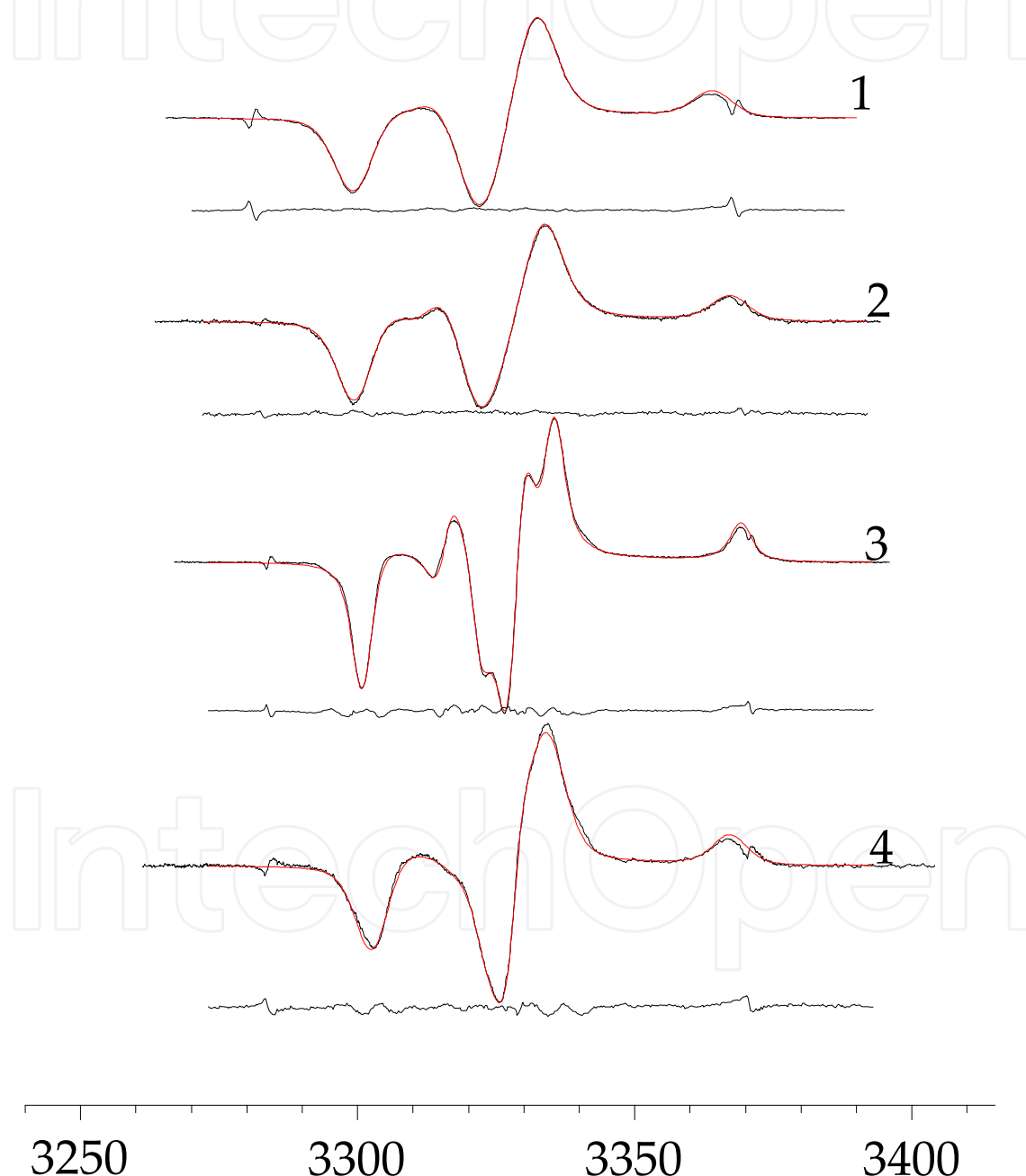


Figure 4. Figure 4. Experimental (black lines) and calculated EPR spectra (red lines) in rigid limit for the systems indicated in Table 4. Below every spectrum, the difference between the experimental and calculated spectra is plotted.

Figure 4 shows the coincidence of the calculated and experimental spectra within the errors of recording. The parameter values determined by means of fitting are collected in Table 4. One can see from that table that the Lorentzian line width at 77K is ordinarily smaller than the Gaussian line width, but the former is not negligible. When the temperature is higher, the Gaussian line width diminishes but the Lorentzian line width rises. It is seen also that the values of A_x and A_y are comparable with the values of the corresponding Gaussian line width; and as a result, they determined with larger errors. In the case of deuterated TEMPOL (row 3 in Table 4), the accuracy of A_x and A_y determination is noticeably higher.

	Systems	g	A	Gaussian linewidth	Lorentzian Linewidth	Discrepancy and error levels
1	TEMPON in AF2400, 77K	2.00885±0.00009 2.00637±0.00008 2.00227	8.13±0.17 3.01±0.40 32.03±0.05	7.38±0.30 7.82±0.16 5.88±0.15	1.66±0.26 0.00±0.27 1.59±0.11	D = 1.4 10 ⁻⁹ Dn = 1.3 10 ⁻¹⁰ Dr = 5.0 10 ⁻¹⁰
2	Probe I in polystyrene, 77K	2.00960±0.00006 2.00638±0.00005 2.002018	7.12±0.11 5.77±0.12 33.61±0.04	5.99±0.16 7.54±0.14 5.01±0.11	1.25±0.16 0.00±0.13 2.01±0.09	D = 9.2 10 ⁻¹⁰ Dn = 4.3 10 ⁻¹⁰ Dr = 1.5 10 ⁻⁹
3	Deuterated TEMPOL in m-tetrahydrofuran, 77K	2.00985±0.00008 2.00612±0.00006 2.002227	6.53±0.04 6.03±0.03 34.15	2.47±0.08 2.97±0.06 2.09±0.07	0.90±0.05 0.30±0.07 1.98±0.04	D = 1.9 10 ⁻⁹ Dn = 7.7 10 ⁻¹¹ Dr = 1.0 10 ⁻⁹
4	Probe V (n=11) in pentyl-cyanobiphenyl (5CB) at 111K	2.00871±0.00006 2.00614±0.00006 2.002144	2.85±0.18 3.70±0.11 32.27±0.06	4.99±0.13 1.86±0.33 4.68±0.17	0.00±0.29 2.57±0.18 1.88±0.11	D = 3.6 10 ⁻⁹ Dn = 6.3 10 ⁻¹⁰ Dr = 1.5 10 ⁻⁹

Table 4. The magnetic parameters and line width characteristics obtained by simulation of some EPR spectra in rigid limit

3.2.4. Quality of simulation and errors of the values defined

The correct measure of the acceptable deviations of the calculated spectrum from the experimental one is the errors of the spectrum recording. In general, there are several sources of experimental errors related to recording of EPR spectra: noise of spectrometer, nonlinear baseline, presence of paramagnetic impurities, etc. Commonly only the noise level of the spectrometer is estimated in experiments and used in the analysis of EPR spectra. This value is the obtained variance of a linear fit to the two baseline segments at either end of the spectrum [5]. Such a value will be designated below as D_n . The more reliable way of estimating error level is reproducing the experiment and calculating the standard deviation between the two spectra according to formula (4). Such value will be denoted as D_r . The value of the experimental errors estimated by reproducing experiment D_r is often up to 10 times larger than the noise level D_n estimated using the outside fragments of the spectrum

(last column on Table 4). Unfortunately, some errors of spectrum recording (presence of paramagnetic impurities, nonlinear field sweep, etc.) are hardly estimated quantitatively. Obviously, ignoring some error sources is the reason why discrepancy in the final point of minimization is somewhat larger than the estimated level of the recording errors.

Comparison of the discrepancy with the error level is a sensitive and reliable characteristic of validity of parameters that vary in the course of the fitting. It is clear that using of an additional fitting parameter is reasonable when the achieved decrease in discrepancy is more than the level of the experimental errors. If the achieved improvement of fitting is less than the error level, the additional parameter should be considered as redundant.

Standard deviation and confidence range for parameter value can be estimated on the basis of the covariance matrix at the minimum point as follows [25]:

$$\sigma_i = \sqrt{c_{ii}}; \quad \delta x_i = \pm t_{n-p}^{\alpha/2} \sqrt{c_{ii}}, \quad (8)$$

where t is the Student coefficient, α is the confidence probability, c_{ii} is the covariance coefficient for the varied parameter x_i .

Such estimation of errors means that the difference between the experimental and calculated spectra, which is caused by imperfection of calculation model, is assumed to be equivalent to noises and other errors of the spectra recording. For unweighted residual minimization, the t distribution statistics is used to estimate the confidence bounds for each parameter [29]. Values of the standard deviations of the determined values are used in what follows as errors of defined values. It should be noted that repeated performance of the experiment and spectrum simulation shows that the errors calculated as described earlier are somewhat underestimated. The calculations of the errors using χ^2 statistics produce the similar underestimated values. The more realistic error of the defined value seems to be the confidence interval for a 99% confidence level (Student's t-distribution coefficient is equal to 2.57).

3.3. EPR spectra in case of librational molecular movements

Rotational mobility is usually considered as one of the simple models: Brownian rotation diffusion, free rotation, or rotational jumps [4,30]. It is known, however, that these models are not sufficient for satisfactory description of EPR spectra in some media. The largest differences between predicted and experimental spectra are observed when the paramagnetic probe is in media with inhomogeneous microstructure, for example, in the liquid crystalline media, on the surface of adsorbents or in polymer matrices. The last case is better studied and is considered in the following section in detail.

3.3.1. Inadequacy of the simple models of motion

The temperature dependence of the EPR spectrum for spin probe 2,2,6,6-tetramethyl-4-oxopiperidine-1-oxyl (TEMPO) in polystyrene (PS) matrix is presented in Figure 5 as an example.

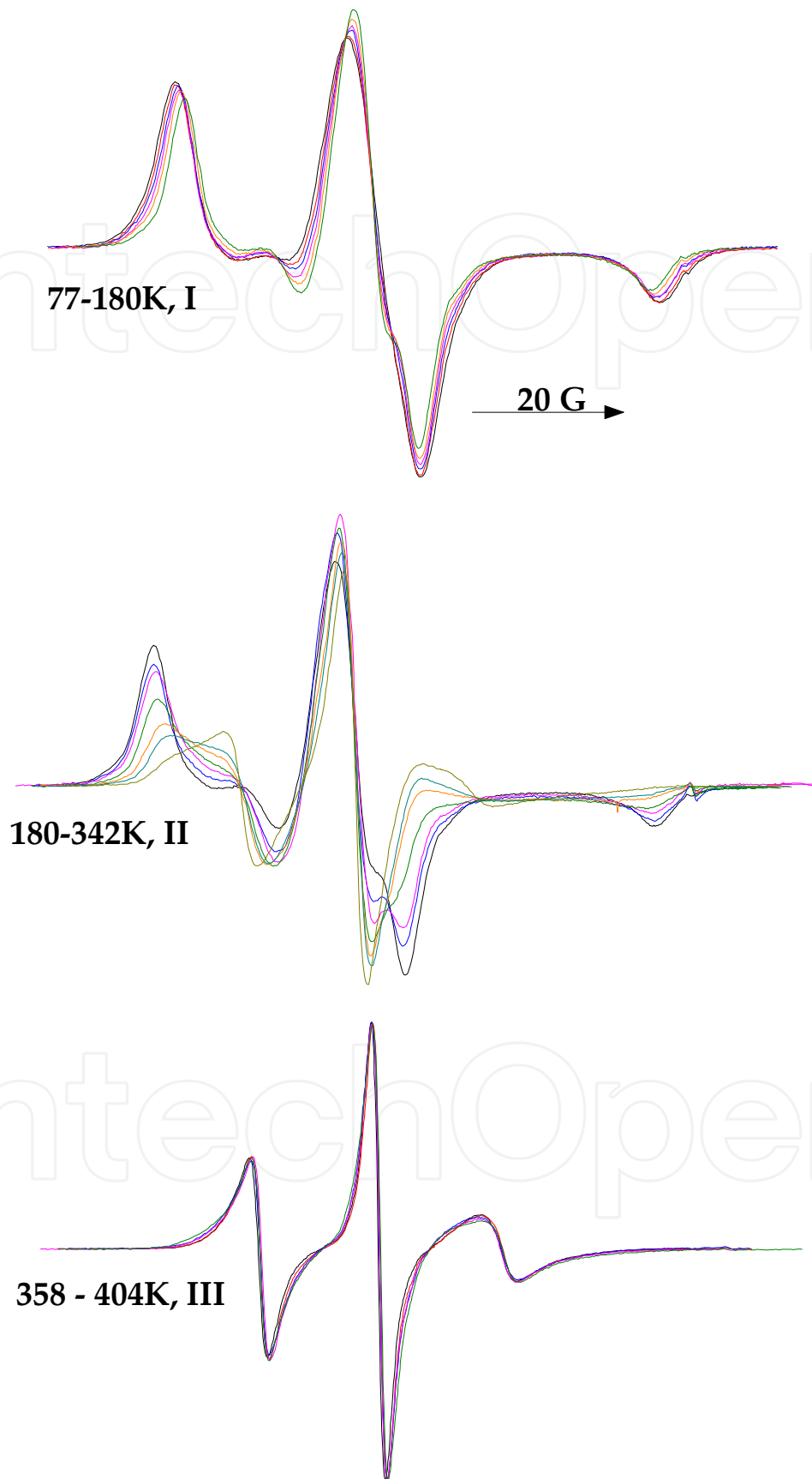


Figure 5. ESR spectra of TEMPON in polystyrene [31].

One can see that when temperature rises, a broad asymmetric spectrum transforms into a narrowed spectrum characterized by motion-averaged magnetic parameters. Increase in rotational mobility results in decrease in separation of the outermost spectral components and diminishing line width. For clarity, all the spectra in Figure 5 are normalized to make the amplitude of the central peak of the spectrum equal to unity. It is seen that the whole temperature dependence of the EPR spectrum in polymer can be divided into three ranges with different specific spectral changes. In the low temperature range (range I, <180 K), the outer extrema of the spectrum smoothly move toward the center as temperature increases. The second range (range II, 180–350K) is characterized by qualitative changes in the shape of the EPR spectrum. A new phenomenon specific for rigid glassy polymers near glass transition temperature is seen in temperature range III (350–405K). In this range, spectral lines narrow, whereas the ratios of amplitudes of different components vary insignificantly. Such spectral behavior is in contradiction with the results of the Redfield relaxation theory [32] and semi-empirical formulas used for analysis of the EPR spectra of paramagnetic probes in liquids [1-3, 33, 34].

The best results of spectra simulation for TEMPON in polystyrene using the model of Brownian diffusion are presented in Figure 6. The deviations far exceeding the experimental errors are seen in this figure for almost the whole temperature range presented. Low-temperature spectra are reproduced rather well, but the rotation correlation times obtained are of the order of 10^{-7} s. This value is in the sharp disagreement with the other measurements, as it will be shown below. The spectra for the middle of the presented temperature range show the qualitative difference with the experimental ones. The above-described specific feature of high temperature spectra, that is, the constancy of the components ratio, is not obtained in the course of fitting.

There are two causes for this disagreement. The first one is the oversimplified model of rotational movements. Today, it is clear that the particle in the polymer medium should be characterized by a wide spectrum of rotations with different frequencies. The most comprehensive model of molecular mobility of the EPR probe in condensed media is the model of slowly relaxing local structure (SRLS) [7, 35], which assumes the fast motions of nitroxide in a matrix cage and the simultaneous slow cage reorientation. If the cage motion is slow enough to be disregarded, SRLS is reduced to the microscopic-order macroscopic-disorder model, which considers nitroxide motion in the potential produced by the cage [36, 37]. In the rigid matrices at low temperatures, the cage barrier exceeds significantly the thermal energy $E_{\text{barrier}} \gg kT$. Then, the values of the angular displacements of nitroxides are restricted, and the motion is turned into librations near equilibrium position.

The second feature that produces troubles in the course of spectra simulation is the distribution of probe molecules according to their mobility. The local surrounding of different probe molecules differs in free volume, molecular alignment, and other conditions. One of the most known examples are the polymers containing crystalline and amorphous areas. As a result, different molecules demonstrate different rotational mobility.

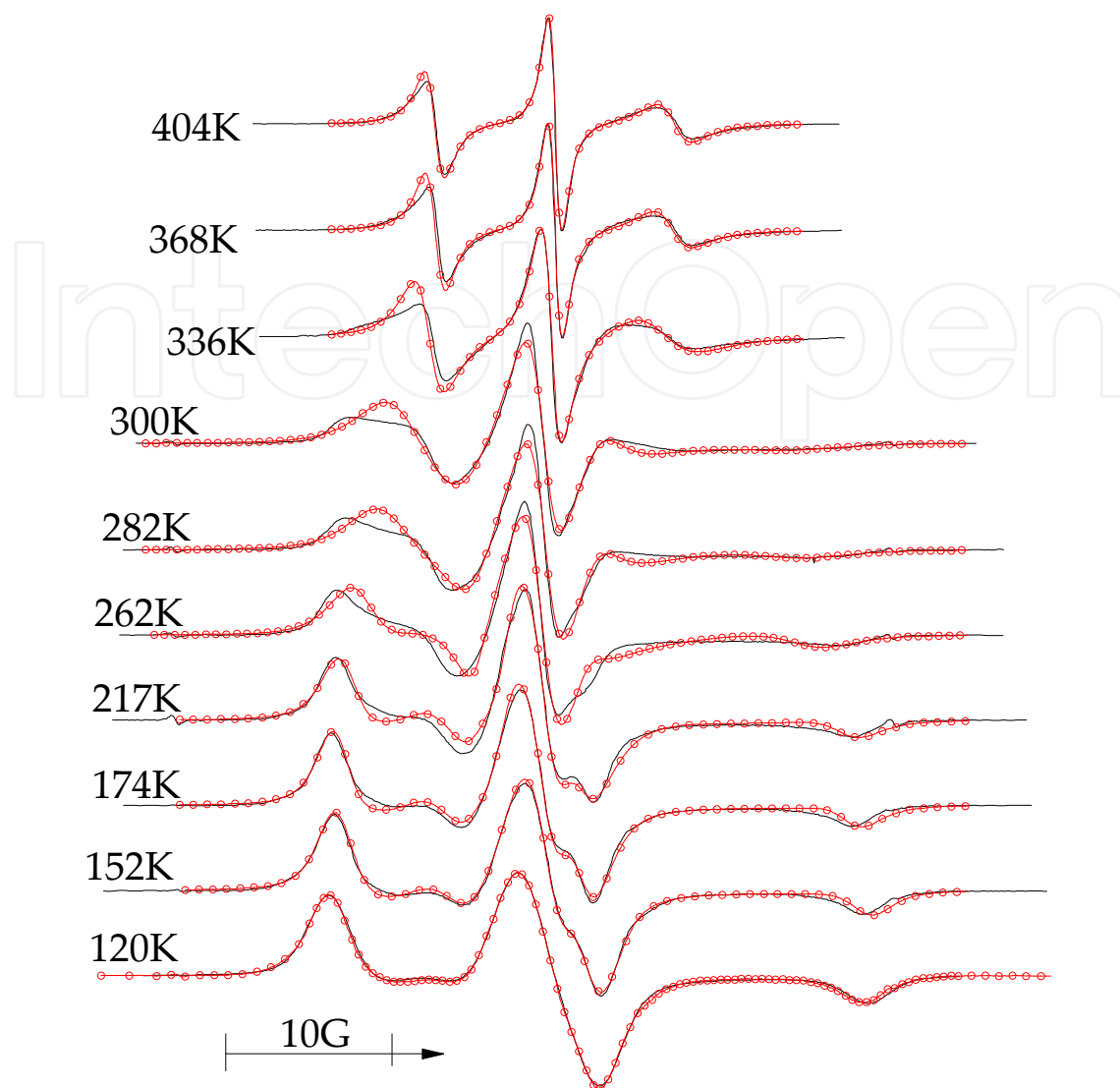


Figure 6. The best fitting of the spectra for TEMPON in polystyrene within the framework of the anisotropic diffusion model.

3.3.2. Concept of molecular quasi-librations [38]

The term “libration” is commonly used for harmonic angular oscillations of molecules in crystals with frequencies of 10^{11} – 10^{12} s^{-1} and amplitudes of approximately 2 – 3° . A similar type of motion in glasses has been evidenced by high-frequency EPR [39], magnetization transfer [40], and spin-echo experiments [41–44]. Librations are averaging motions in time scale of EPR. The sensitivity of the EPR method to angular displacements with different frequencies is qualitatively illustrated in Figure 7.

The figure presents the time required for the rotational displacement on the angle specified on the abscissa. This dependence characterizes the molecular mobility in the medium. The range of frequencies and corresponding amplitudes that influence the X-band EPR spectrum are shown in Figure 7 as a sensitivity window. The window is shifted to higher frequencies when high-frequency EPR spectroscopy is used.

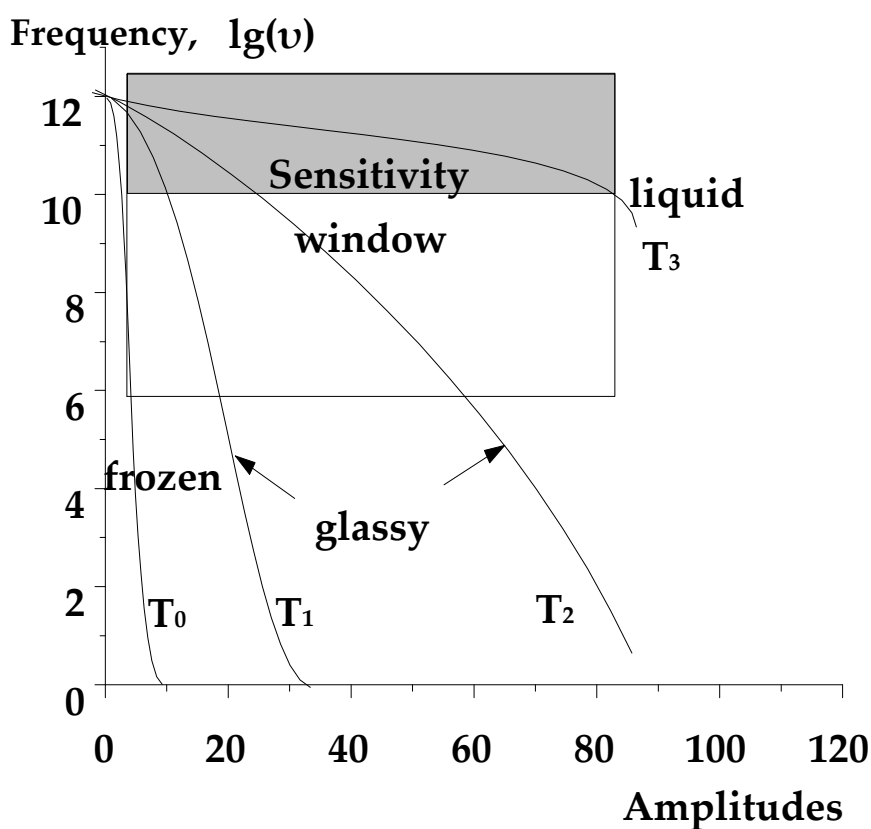


Figure 7. Relaxation curves typical for different states of matter ($T_0 < T_1 < T_2 < T_3$).

In Figure 7, the curve marked T_0 corresponds to a solid sample at a low temperature. The molecular motions possible in such conditions do not fall into the sensitivity window and, thus, do not change the EPR spectrum (rigid-limit conditions). The curve T_3 corresponds to the liquid sample with low viscosity. Any angular displacement of the probe in such medium requires the time less than 10^{-10} s. It is known that such rotations fully average the magnetic parameters of the nitroxide probe. It means that EPR spectrum recorded in these conditions consists of components corresponding to averaged g value (\bar{g}) and averaged hyperfine constant \bar{A} . Rotational mobility shows itself in such spectra in width and amplitudes of spectral components and can be estimated using the Redfield relaxation theory [32, 33]. The area of averaging movements is marked in Figure 7 by the gray color.

There are many systems in which small angular displacements proceed with averaging frequencies in EPR time scale, but greater displacements that require larger time do not average magnetic parameters (curves T_1 and T_2 in Figure 7). These conditions are ordinary, for example, in cases of glassy polymers or paramagnetic labels attached to large biomolecules. In these cases, the magnetic parameters of probe or label are averaged only partially. The set of movements with frequencies that are averaging in the EPR time scale are not limited to harmonic vibrations near the equilibrium position but comprises combined movements of the local probe surrounding. It means that these movements can be stochastic and of higher amplitude than ordinary librations in crystals. To draw a distinction

between ordinary librations in crystals and stochastic librations of spin probe in glasses, the latter should be referred to as “quasi-librations.”

Partial averaging of the probe magnetic parameters by the movement with high-frequency but limited amplitude was considered earlier in [45, 46]. On the basis of these works, it can be shown [47] that the following averaging formulas are valid in the case of quasi-librations around three g-tensor axes simultaneously:

$$\begin{aligned} \langle A_x \rangle &= A_x + 0.5(A_z - A_x)(1 - P_y) + 0.5(A_y - A_x)(1 - P_z) \\ \langle A_y \rangle &= A_y + 0.5(A_z - A_y)(1 - P_x) + 0.5(A_x - A_y)(1 - P_z) \\ \langle A_z \rangle &= A_z + 0.5(A_x - A_z)(1 - P_y) + 0.5(A_y - A_z)(1 - P_x) \end{aligned} \quad (9)$$

where $P_x = (\sin L_x \cdot \cos L_x) / L_x$, $P_y = (\sin L_y \cdot \cos L_y) / L_y$, $P_z = (\sin L_z \cdot \cos L_z) / L_z$;

$\langle A_x \rangle$, $\langle A_y \rangle$, $\langle A_z \rangle$ and A_x , A_y , A_z are averaged and intrinsic hyperfine constants, respectively;

L_x , L_y , and L_z are half-amplitudes of the motion around the X, Y, and Z axes, respectively.

It should be noted that equation (9) uses the assumption of independency of quasi-librations around different axes. As a result, the equation is applicable for any quasi-libration amplitudes in the case of movements around a single axis. In the case of simultaneous quasi-librations around three axes, this assumption is valid at small amplitudes only (less than approximately 45°).

Some authors use mean-squared sine of the displacement angle averaged over all the paramagnetic particles, $\langle \sin^2 \alpha_x \rangle$, $\langle \sin^2 \alpha_y \rangle$, and $\langle \sin^2 \alpha_z \rangle$, for characterization of quasi-libration motion [43, 44, 48-50]. The relations between these characteristics and the quasi-libration amplitudes mentioned earlier are given by

$$\begin{aligned} \langle \sin^2 a_x \rangle &= 0.5(1 - P_x) = 0.5 \left[1 - (\sin L_x \cdot \cos L_x) / L_x \right] \\ \langle \sin^2 a_y \rangle &= 0.5(1 - P_y) = 0.5 \left[1 - (\sin L_y \cdot \cos L_y) / L_y \right] \\ \langle \sin^2 a_z \rangle &= 0.5(1 - P_z) = 0.5 \left[1 - (\sin L_z \cdot \cos L_z) / L_z \right] \end{aligned} \quad (10)$$

By using the averaged mean-squared sine of displacements, equations (9) transforms into the following:

$$\begin{aligned} \langle A_x \rangle &= A_x + (A_z - A_x) \langle \sin^2 a_y \rangle + (A_y - A_x) \langle \sin^2 a_z \rangle \\ \langle A_y \rangle &= A_y + (A_z - A_y) \langle \sin^2 a_x \rangle + (A_x - A_y) \langle \sin^2 a_z \rangle \\ \langle A_z \rangle &= A_z + (A_x - A_z) \langle \sin^2 a_y \rangle + (A_y - A_z) \langle \sin^2 a_x \rangle \end{aligned} \quad (11)$$

The average expressions for the case of arbitrary direction of quasi-libration axis in g-tensor frame are presented in [51, 52]:

$$\begin{aligned}
\langle A_x \rangle &= k_1 A_x + 2k_2 c_1^2 A_x + k_3 (c_1^2 A_x + c_2^2 A_y + c_3^2 A_z) c_1^2 + k_4 (c_2^2 A_z + c_3^2 A_y) \\
\langle A_y \rangle &= k_1 A_y + 2k_2 c_2^2 A_y + k_3 (c_1^2 A_x + c_2^2 A_y + c_3^2 A_z) c_2^2 + k_4 (c_3^2 A_x + c_1^2 A_z) \\
\langle A_z \rangle &= k_1 A_z + 2k_2 c_3^2 A_z + k_3 (c_1^2 A_x + c_2^2 A_y + c_3^2 A_z) c_3^2 + k_4 (c_2^2 A_x + c_1^2 A_y),
\end{aligned} \tag{12}$$

where c_1 , c_2 , and c_3 are the direction cosines of the quasi-libration axis, $k_1 = 0.5(1 + \sin 2L / 2L)$, $k_2 = \sin L / L - k_1$, $k_3 = 1 - 2\sin L / L + k_1$, $k_4 = 0.5(1 - \sin 2L / 2L)$, and L is the half amplitudes of motion around the libration axis.

The expressions for the averaged g-tensor components are analogous to that presented for hfi-tensor.

The quasi-libration concept essentially divides molecular rotational movements into two kinds: high and low frequencies. Similar differentiation lies on the basis of the known SRLS model [7, 35]. Thus, the quasi-libration concept is the simplified version of the SRLS model. Both models describe the frequency and amplitude distribution of rotational movements of one paramagnetic center and assume that all probe molecules in the sample demonstrate the identical molecular mobility. On the other hand, it is known that real systems often show clear microscopic inhomogeneity that induces the difference in mobility of different particles as a result of variation of local structure [34, 39, 53-56]. Thus, generally, both distributions: distribution characterizing the different movements of one particle and distribution of particles, should be taken into account for adequate description of EPR spectra.

3.3.3. Low temperature range of temperature dependence

Figure 5 shows that at low temperatures, the EPR spectra of nitroxides (temperature range I) slowly change as the temperature increases and retain shape typical for rigid limit. This set of spectra can be successfully described using different models of rotation mobility, particularly within the model of Brownian diffusion, jump rotation, quasi-librations, and the rigid-limit model with some changed magnetic parameters. Thus, the changes in spectrum in this temperature range are model insensitive. The choice of an adequate model in this situation should be based on additional data obtained using other experimental techniques. The simulation of spectra in range I within the models of Brownian rotation diffusion and jump rotation leads to the conclusion that the rotation correlation time of admixture molecules in glassy polymers noticeably below the glass transition point lie in the range 10^{-6} – 10^{-7} s. Such rapid rotation in solid media at a low temperature seems to be quite unrealistic. Experimental measurements of rotational relaxation times by means of light induced alignment of nitroxides [48, 49] give for glassy polystyrene characteristic values approximately 10^1 – 10^3 s for room temperature. It means that rotation correlation time estimated from the analysis of the EPR spectrum within the Brownian rotation model exceeds the real value by 10 orders of magnitude. This contradiction leads us to conclude that only the model of quasi-librations with limited amplitudes adequately describes the real molecular rotations in range I.

The fitting of experimental spectra in the framework of the quasi-libration model included the variation of quasi-libration amplitudes and width of individual resonance line. The magnetic parameters of the probes were obtained by simulation of rigid-limit spectra and were not further changed. The results of the fitting of the EPR spectra in the temperature range I are presented in Figure 8(a).

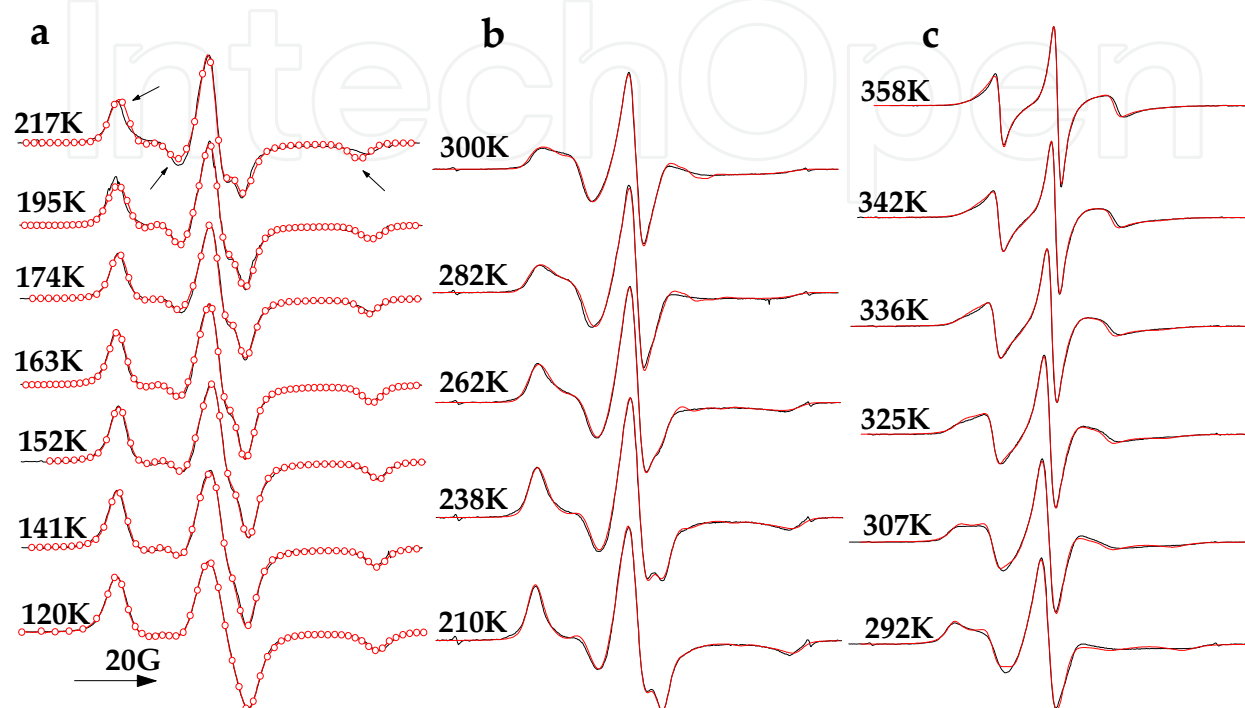


Figure 8. Experimental (black lines) and calculated EPR spectra (red lines) for TEMPON in polystyrene: (a) quasi-libration model, (b) Gaussian distribution of quasi-libration amplitudes, and (c) quasi-librations and lognormal distribution of rotation correlation times.

One can see from Figure 8a that satisfactory agreement between the experimental and calculated spectra holds up to a temperature of approximately 200K. One can see that the spectrum at 217K cannot be qualitatively reproduced taking into account the simple quasi-librations. At higher temperatures, the deviations of the calculated spectra from the experimental ones become larger still.

In the course of fitting, it was found that the amplitudes of quasi-librations around different molecular axes are determined with different accuracy. In particular, the amplitudes of movements around the z-axis are defined with uncertainty as approximately 10° . In this connection, for description of the presented experimental spectra, it was possible to assume the uniaxial symmetry of quasi-librations, namely, amplitudes for the y and z axes being equal: $L_y = L_z = L_{yz}$.

3.3.4. Distribution of quasi-libration amplitudes [47]

For quantitative description of the spectra recorded at higher temperatures, the distribution of the probe molecules according to their libration amplitudes should be taken into account.

We tried to describe the experimental spectra using three different distribution functions: rectangular, bimodal, and Gaussian distributions. The fitting procedure was found to be rather sensitive to the distribution shape. We have not achieved positive results when the rectangular distribution was used. The bimodal distribution was found to be useful only in the case of porous Teflon AF2400. Obviously, it is a result of the specific structure of this polymer, which is characterized by bimodal distribution of microstructure. An annihilation positron study shows that free volume distribution in AF2400 has a bimodal shape [57]. In the cases of conventional polymers, using the Gaussian distribution of quasi-libration amplitudes permits to expand the temperature range of quantitative simulation of the spectra shape. Figure 8(b) demonstrates as an example the coincidence of experimental and calculated spectra of TEMPON in polystyrene up to room temperature.

The temperature evolution of the distribution is presented in Figure 9. One can see a graduate shift of the distribution to higher quasi-libration amplitudes and narrowing of the distribution when the temperature increases. The temperature dependencies of averaged quasi-libration amplitudes for TEMPON in different polymers are presented in Figure 10. The difference in these dependencies reflects different properties of polymer matrices. The clear dependence of quasi-libration amplitudes on the probe molecular size is detected as well.

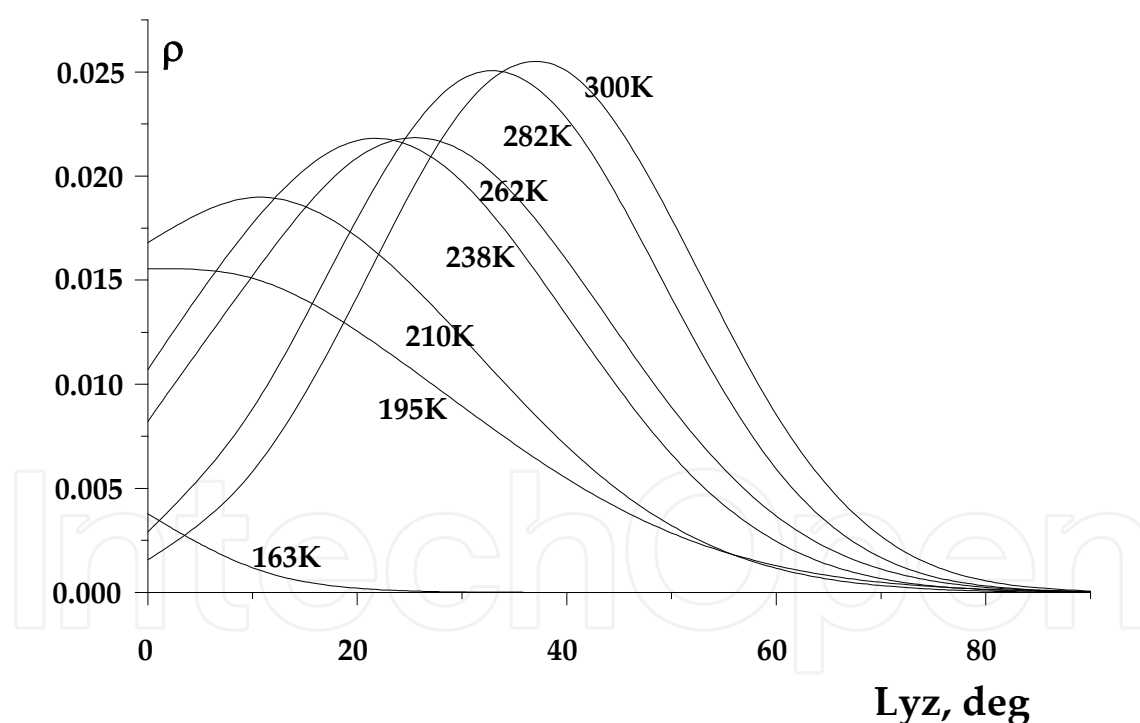


Figure 9. Shape of the Gauss distribution for TEMPON in PS.

It is seen from Figures 9 and 10 that when the averaged quasi-libration amplitude reaches 40–50° the high-amplitude tail of the distribution spread to 90°. The quasi-librations with this amplitude cannot be distinguished from rotational movements. It is not surprising, therefore, that EPR spectra at higher temperatures cannot be simulated within the framework of the quasi-libration model only.

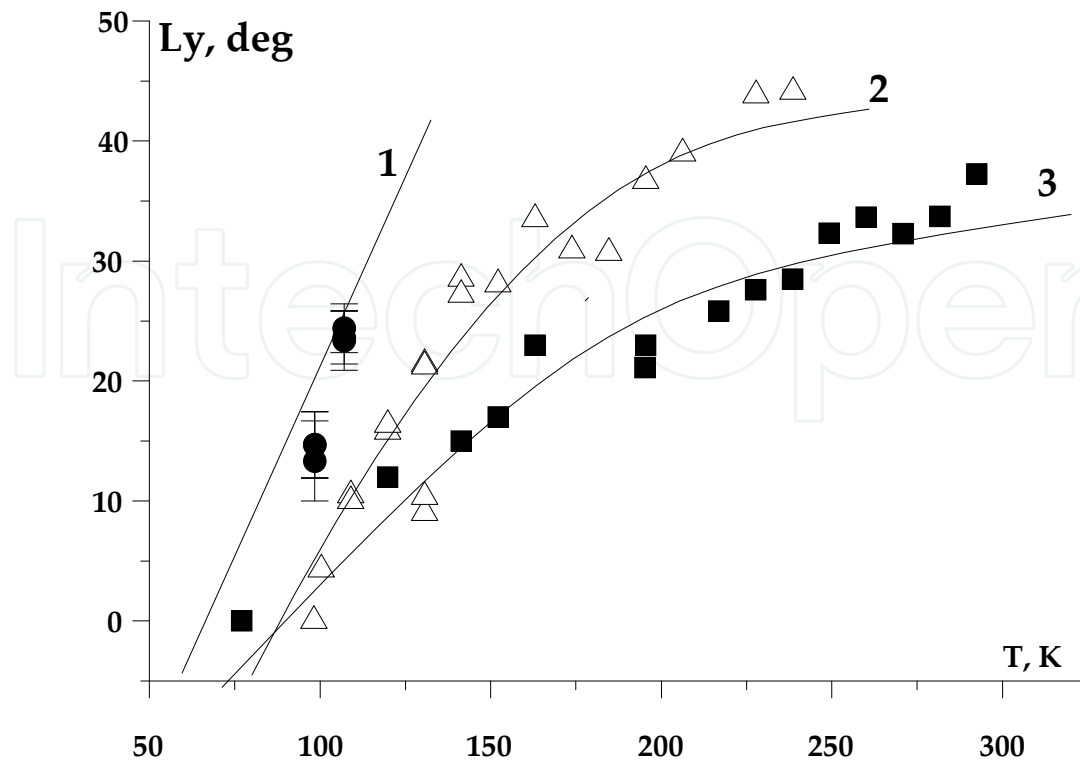


Figure 10. Quasi-libration amplitudes of TEMPN in AF-2400 (1), PVTMS (2), and PS (3).

3.3.5. Quasi-libration and rotational diffusion

At a temperature higher than 300K, the EPR spectra of TEMPN in polystyrene cannot be qualitatively described using the Brownian rotation diffusion (Figure 6) or quasi-librations only. Both these movements should be taken into account simultaneously. This model assumes that the probe takes part in two types of motion: fast quasi-librations restricted by the matrix cage and slow Brownian diffusion caused by the cage rearrangement. The difference in the cage properties can be taken into account by means of log-normal distribution of correlation times for cage reorientation:

$$\rho(R) = \begin{cases} 0, & R < 0 \\ \frac{1}{\sigma\sqrt{2\pi}} \exp\left(-\frac{(\ln R - \ln R_0)^2}{2\sigma^2}\right), & R > 0 \end{cases} \quad (13)$$

where R is the rotational diffusion coefficient and $\ln R_0$ and σ are the center and dispersion of the distribution, respectively.

Application of this combined model gives satisfactory agreement between calculated and experimental spectra in the high temperature range (Figure 6(c)). It should be pointed out that taking into account quasi-librations is a necessary requirement for satisfactory description of these spectra. The average correlation time for cage reorientation obtained as results of spectra

simulations was found to be approximately 10^{-7} s at 360K. Characteristic widths of the distributions lie in the range of 0.6–1.0 decades. The obtained data conform to the literature data on the width of distribution of correlation times in polymers [56, 58-60]. The distribution narrows when temperature rises. Our calculations show that the distribution with a width of 0.4 decades or smaller does not influence the simulated ESR spectra.

The presented consideration shows that by using the quasi-libration model and taking into account the molecular distributions, it is possible to describe within experimental accuracy the EPR spectra of paramagnetic probe in polymer matrix in the whole temperature range near and below the glass transition point. The examples of some other polymers are presented in [38, 47].

3.3.6. Correlation between molecular mobility and reaction rate [61]

Having the opportunity to obtain detailed characteristics of rotational mobility of admixture molecules in polymer matrix, it is interesting to examine the influence of rotation mobility on the molecular reactivity. For this purpose, we used four bifunctional probe molecules carrying a paramagnetic nitroxide fragment and a photochromic azobenzene moiety (Figure 3). The azobenzene fragment of these molecules is known to undergo photochemical *trans*-to-*cis* isomerization [62]. The kinetic curves of photo-isomerization of probe II in polystyrene matrix are presented in Figure 11 as an example.

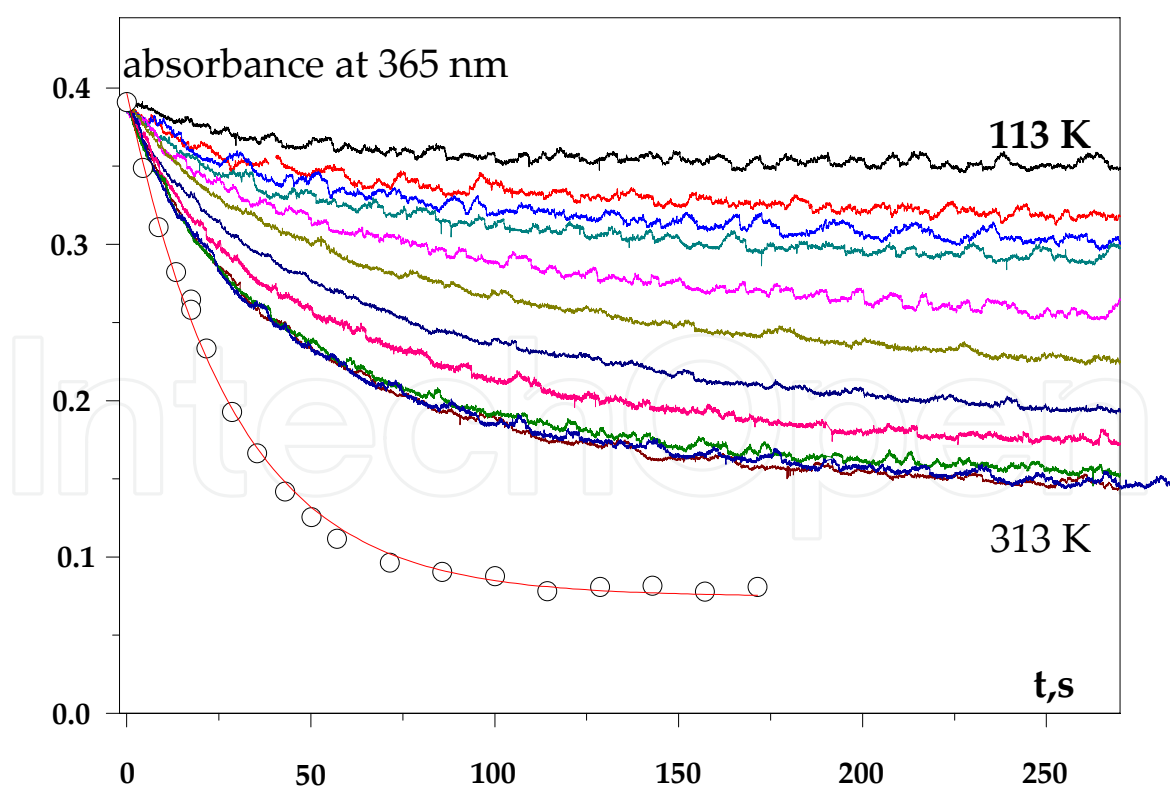


Figure 11. Kinetic curves of *trans*-*cis* photo-isomerization of probe II in glassy polystyrene and in solution (points).

As one can see, the influence of the polymer media consists in diminishing photoreaction rate (reduction of reaction quantum yield) and lowering the reaction yield at prolonged irradiation. Both these effects are the results of restriction imposed by the matrix on molecular rearrangement. The less extent of the photoreaction indicates that some fraction of initial trans-isomer is incapable of the reaction as a result of the rigid matrix surrounding. This conclusion was proven by the following experiment (Figure 12). The sample was irradiated at a low temperature until photoreaction has almost stopped. Then the sample was annealed at room temperature in the dark and cooled to the initial low temperature. Such annealed sample demonstrated recovered high rate of photoreaction at irradiation.

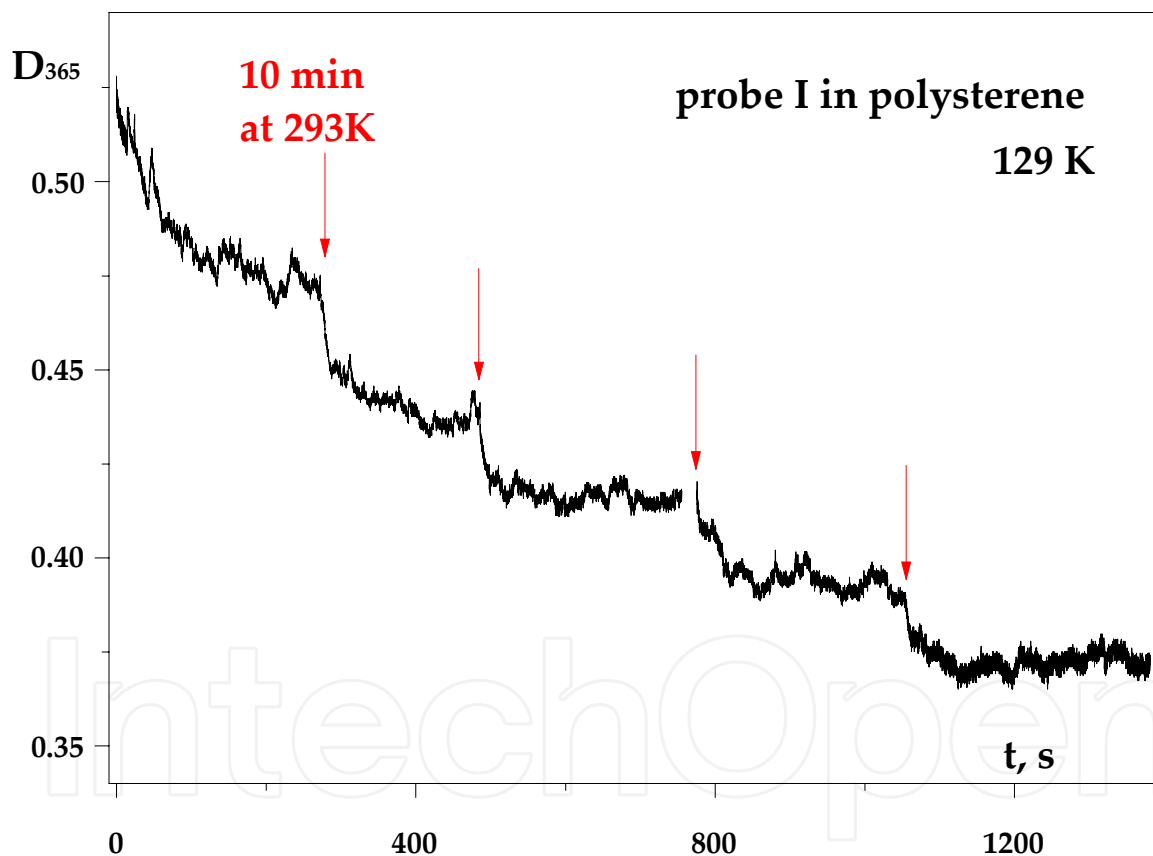


Figure 12. The kinetics of photoreaction of probe I in polymer media at 129K, which was interrupted in pointed moments, and the sample was annealed 10 minutes at 293K without light irradiation.

Determination of the quasi-libration amplitudes was performed by numerical simulation of the EPR spectra as described earlier. The obtained amplitudes are collected in Figure 13. In accordance with the molecular geometry, the largest amplitudes are detected for quasi-libration around the longest molecular axis (x -axis of the g -tensor).

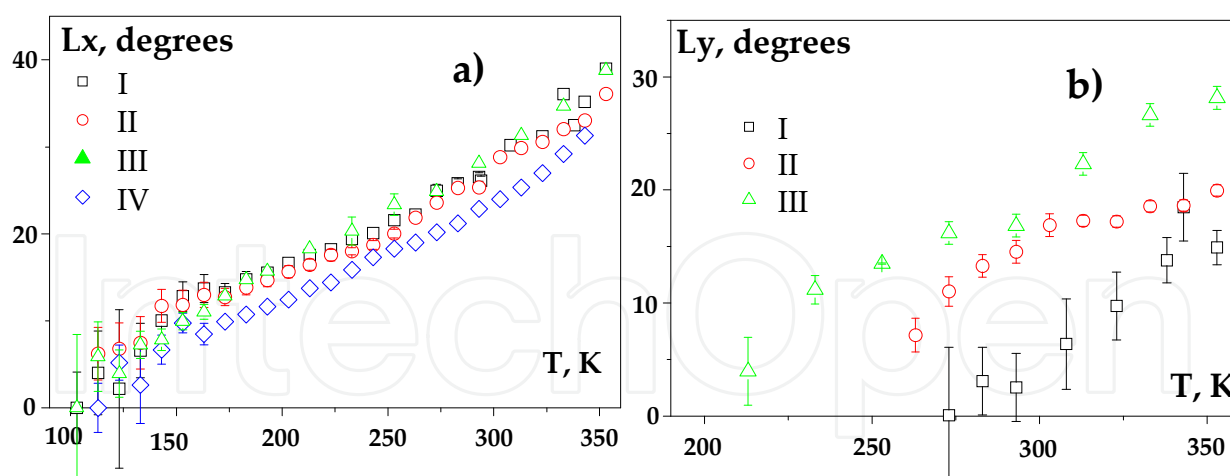


Figure 13. Averaged values of the quasi-libration amplitudes around axes x (a) and y (b), determined in the course of the numerical simulation of ESR spectra, probes I-IV.

The obtained values of quasi-libration amplitudes can be confronted with the quantum yields of photo-isomerization. The very good correlation of these values is illustrated by Figure 14.

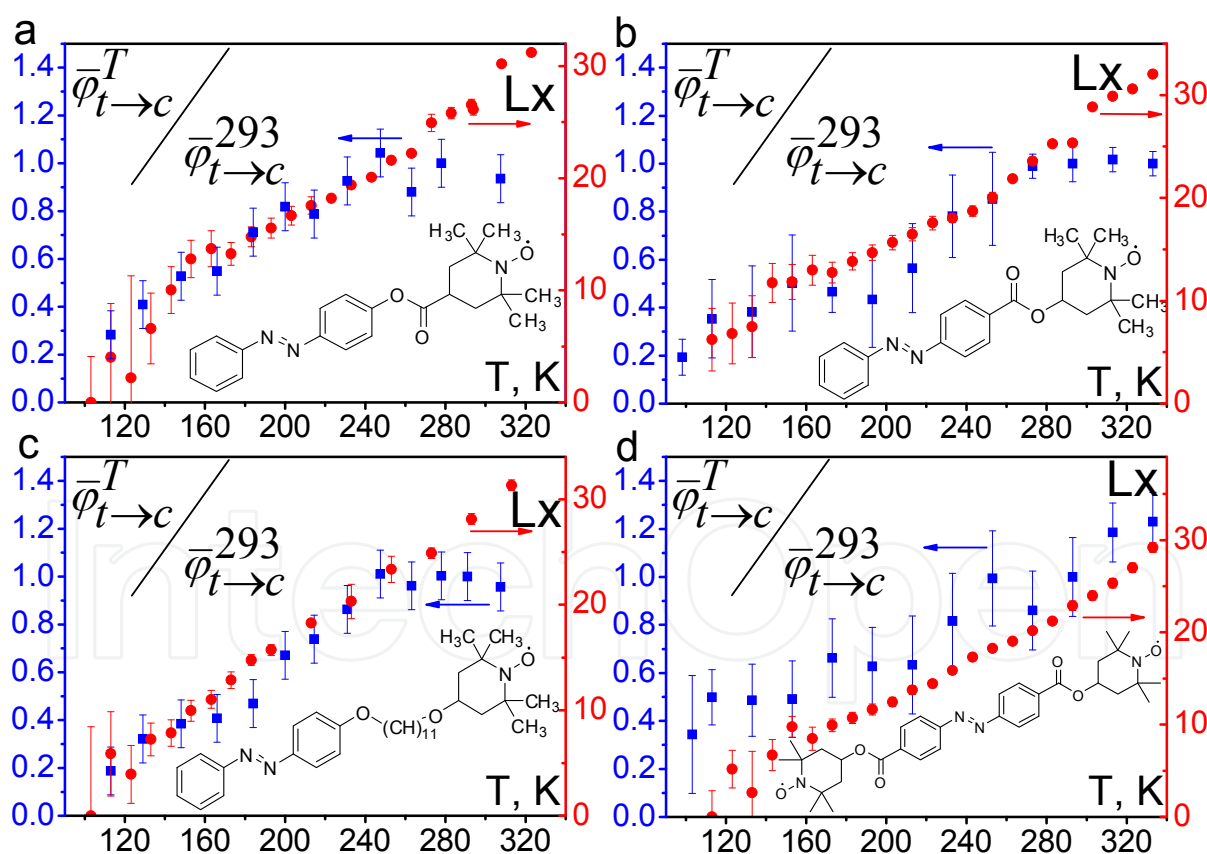


Figure 14. Quantum yields of *trans-cis* photo-isomerization and amplitudes of quasi-librations versus temperature.

Even more interesting is the comparison of quasi-libration distributions with the extent of reaction. The Gaussian distribution functions of quasi-libration amplitudes are presented in

Figure 15. Hatched areas denote the fraction of molecules, which are able to undergo photochemical isomerization. The fraction of active molecules in this figure was determined from the results of photochemical experiments. It is seen that the threshold of reactivity for different temperatures is observed at the same quasi-libration amplitude. This value amounts to approximately 10° and can be rationalized by consideration of displacements required for the elementary act of reaction.

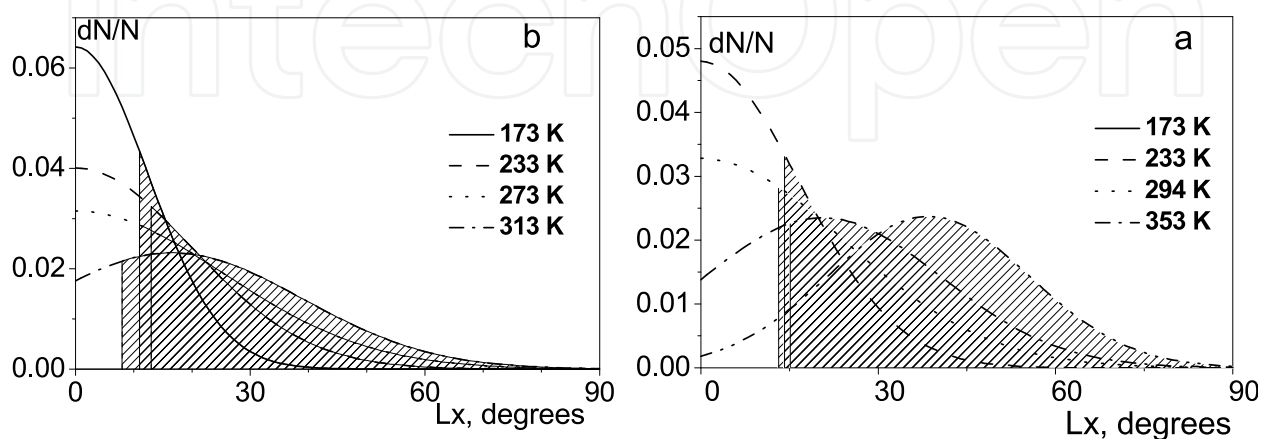


Figure 15. Temperature dependence of the distribution density of the quasi-libration amplitudes for probes I (a) and IV (b), determined as a result of the numerical simulation of the ESR spectra; hatching indicates photo-chemically active molecules.

Thus, the model of quasi-librations and characteristics of molecular displacements in polymer matrix determined by simulation of the EPR spectra are confirmed by kinetic chemical experiments.

4. Orientational alignment of paramagnetic molecules in a sample

Properties of many materials, such as stretched polymers, liquid crystals, and LB-films, are determined by the orientational order of molecules. The most precise characteristic of the molecular order is the orientation distribution function $\rho(\alpha, \beta, \gamma)$, which shows the number (or fraction) of molecules oriented in the angular interval $\alpha + d\alpha, \beta + d\beta, \gamma + d\gamma$, where α, β, γ are Euler angles connecting the molecular reference frame with the sample frame. Information about the characteristics of orientation distribution function is contained in the EPR spectra of nitroxide probe introduced into the ordered medium. The anisotropy of the medium manifests itself in the dependence of spectrum shape on the orientation of the sample respective to the direction of the magnetic field of the spectrometer. Most often, this information was obtained using any assumption about the shape of orientation distribution function. By means of comparison of the calculated and experimental spectra, researchers found the parameters of a priori defined function [4-11, 63-69].

In the present chapter, we describe the model-free method of determining of orientation distribution function [70-76]. The method is based on the expansion of the determined function in a series of orthonormal functions with variable coefficients. The expansion

coefficients are determined through minimization of discrepancies between simulated and experimental spectra.

4.1. Orientation distribution function

In the general case, the orientation distribution function is represented as a series of Wigner functions:

$$\rho(\alpha, \beta, \gamma) = \sum_{j, m', m} \frac{2j+1}{8\pi^2} \langle D_{m'm}^{j*} \rangle D_{m'm}^j(\alpha, \beta, \gamma) \quad (14)$$

However, depending on the symmetry of the system under consideration, the representation of the function can be simplified. When uniaxial molecules form a uniaxial sample, the orientation of each molecule in the sample is uniquely determined by the angle between the anisotropy axis of this molecule and the symmetry axis of the sample. In this case, the orientation function is the function of only one angle $\rho = \rho(\beta)$ and can be represented as a series of Legendre polynomials. When uniaxial paramagnetic particles are arbitrarily distributed in the sample, the orientation of each particle is determined by two angles that characterize the orientation of the anisotropy axis of the particle in the reference frame associated with the sample. In this case, orientation function is a function of two angles $\rho = \rho(\beta, \gamma)$. In a uniaxial sample, the distribution function of particles characterized by three different principal values of g-tensor and/or hfi tensor is also a function of two angles. In this case, the angles β, γ characterize the orientation of the symmetry axis of the sample in the reference frame associated with a paramagnetic particles. The orientation distribution function in these two cases can be presented as a series of spherical harmonics:

$$\rho(\beta, \gamma) = \frac{1}{2\pi} \sum_{j=0}^{\infty} \left(\frac{1}{2} a_{j0} P_j(\cos \beta) + \sum_{m=1}^j P_{jm}(\cos \beta) [a_{jm} \cos m\gamma + b_{jm} \sin m\gamma] \right) \quad (15)$$

where P_j are Legendre polynomials and P_{jm} are associated Legendre functions.

In practice, axially symmetrical samples are studied most often, but magnetic parameters of spin probes possess ordinary orthorhombic symmetry. Hence, the orientation distribution function usually can be represented as series (15). Coefficient a_{00} reflects the full number of radicals; for a normalized orientation function, it is equal to unity.

To characterize the orientation alignment of the uniaxial system, the order parameters are used:

$$\begin{aligned} A_m^j \equiv S_{jm} &= \frac{\langle D_{0m}^{j*} \rangle + \langle D_{0-m}^{j*} \rangle}{2} = \frac{a_{jm}}{2j+1} \sqrt{\frac{(j+m)!}{(j-m)!}} \\ B_m^j &= \frac{\langle D_{0m}^{j*} \rangle - \langle D_{0-m}^{j*} \rangle}{2i} = \frac{b_{jm}}{2j+1} \sqrt{\frac{(j+m)!}{(j-m)!}} \end{aligned} \quad (16)$$

Specification of all the order parameters or all the coefficients in expansions (14) and (15) gives a complete specification of the orientation distribution function. To date, there is no technique for complete experimental determination of an orientation distribution function for soft matter. Only the second moments of orientation function (order parameters of rank two) are determined usually, as they can be obtained using one-photon optical methods. Orientation characteristics of rank four and higher are determined extremely rarely. The EPR spectroscopy of the spin probes and labels provides, in principle, the possibility of complete determination of an orientation distribution function.

For computer realization of the suggested method, the homemade program ODF3 was worked out. This program allows to calculate the series of EPR spectra recorded at various orientations of the sample in the magnetic field of the spectrometer and to determine the characteristics of orientation distribution function in the course of the minimization procedure. A brief description of the program ODF3 is presented in the appendix.

It is necessary to note that orientation function determined by the analysis of EPR spectra is always symmetric with respect to the center of coordinates. Indeed, at turning the magnetic field direction by 180° , the EPR spectrum does not change, and so some unequal orientations of the paramagnetic particle are indistinguishable by EPR. This limitation equally concerns all methods, which use EPR spectroscopy for the study of orientation order. Unfortunately, researchers often do not take this circumstance into account at interpretation of their results. This limitation imposes constraints on the expansion coefficients. When orientation distribution function is represented in the form of Eq. (15), all the coefficients a_{jm} , b_{jm} with odd j are equal to zero.

4.2. Determination of orthorhombic orientation distribution function

The application of the suggested method is demonstrated below on the examples of spin probes in liquid crystals, polymer matrices, and supercooled glasses [73-77].

In Figure 16(a), one can see some EPR spectra of the standard spin probe TEMPOL (Figure 3) in nematic liquid crystal 5CB (4-*n*-amyl-4'-cyanobiphenyl) aligned by the magnetic field of the EPR spectrometer [73,74]. The spectra were recorded at $T = 77\text{K}$ (in liquid nitrogen) at various angles between the symmetry axis of the sample and the magnetic field of the EPR spectrometer. The angular dependence of the spectrum shape proves that the paramagnetic molecules are partially ordered by the liquid crystal. In Figure 16(b), the result of the joint simulation of these spectra is presented. Here, as well as in other examples, the magnetic parameters of the radical were determined previously by means of simulation of the spectrum of isotropic sample. Hence, in the course of simulation of the angular dependence, only expansion coefficients of the orientation function were varied.

Because in EPR spectroscopy there is no principal prohibition for determination of the high-rank-order parameters of the orientation function, we simulated the series of EPR spectra several times with consecutive increases in the expansion order. When adding expansion members of the next order did not lead to improvement of the description of the

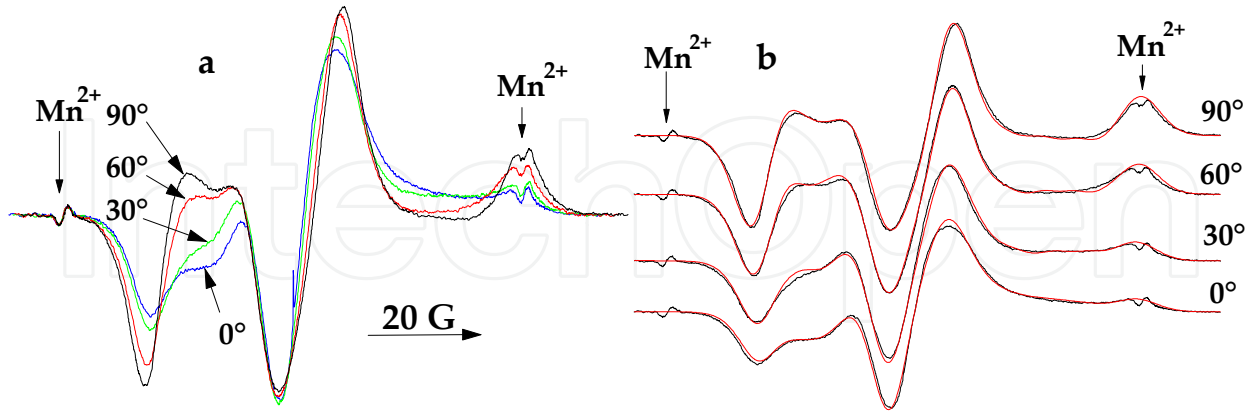


Figure 16. EPR spectra of TEMPOL in aligned liquid crystal 5CB recorded at different angles between the magnetic field vector and the sample director.

experimental spectra we supposed that the next coefficients are close to zero within the errors of determination. The result of simulation of the spectra is shown in Figure 16(b). The values of the coefficients are presented in Table 5. It was found that the expansion coefficients of the second and fourth orders are determined reliably.

The orientation distribution function of TEMPOL in 5CB is presented in Figure 17(a). The function describes the orientation distribution of the sample director in the frame of paramagnetic molecule. The principal axes of the g -tensor are used as coordinate axes. The orientation of these axes in the nitroxide radical is shown in Figure 17(b). From Figure 17(a), one can see that the TEMPOL magnetic axis Z is oriented predominantly perpendicular to the sample symmetry axis. Possibly, it is a result of the interaction of the electron pairs of nitrogen and oxygen atoms with the π -system of the benzene ring of the liquid crystal molecules. The X and Y axes of the TEMPOL molecules are predominantly directed at 50° and 40° to the sample anisotropy axis, respectively. The corresponding orientation of the molecules of spin probe and liquid crystal is shown in Figure 17(b).

It is necessary to emphasize that in the presented case, the orientation distribution function possesses orthorhombic symmetry. The principal axes of the g -tensor and hfi-tensor practically coincide in the case of TEMPOL and other nitroxide radicals. It means that nitroxide probes have orthorhombic symmetry. Since the effective values of the magnetic parameters are defined by squares of the directional cosines of the magnetic field vector in the g -frame and hfi-frame correspondently (17), eight different molecular orientations are undistinguishable by EPR.

$$g_{eff}^2 = g_{xx}^2 \cos^2(HX_g) + g_{yy}^2 \cos^2(HY_g) + g_{zz}^2 \cos^2(HZ_g) \quad (17)$$

$$A_{eff}^2 = A_{xx}^2 \cos^2(HX_A) + A_{yy}^2 \cos^2(HY_A) + A_{zz}^2 \cos^2(HZ_A) \quad (18)$$

System	a_{20} a_{40} a_{60}	a_{21} b_{21}	a_{22} b_{22}	a_{42} a_{44}	a_{62} a_{64} a_{66}
TEMPOL in 5B	-0.872 ± 0.007 0.247 ± 0.015 –	– –	0.082 ± 0.004 –	-0.0004 ± 0.0012 -0.0047 ± 0.0003	– – –
V(n=11) in 5CB	1.91 0.11 –0.70	– –	–0.133 –	–0.065 ~0	–0.024 ~0 ~0
V(n=11) in 5CB/pores	1.35 0.21 –	– –	–0.18 –	–0.010 –0.0006	– – –
V(n=4) in stretched PE	0.82 – –	– –	–0.029 –	– –	– – –
V(n=11) in stretched PE	1.43 0.37 –	– –	–0.106 –	–0.018 –0.0016	– – –
V(n=15) in stretched PE	2.42 1.06 0.144	– –	–0.103 –	–0.056 0.0011	–0.0016 ~0 ~0
VI in stretched PE	0.49 0.22 –	– –	–0.056 –	–0.010 ~0	– – –
HO ₂ in glassy H ₂ O ₂	0.25 – –	0.073 0.181	0.025 0.038	– –	– – –
Cl ₂ [•] in glassy LiCl (5mol/l)	–0.25 – –	– –	– –	– –	– – –

Typical errors of values determined are presented in the first row of the table.

Table 5. The expansion coefficients of series (15) for the orientation distribution functions of some radicals in different matrices

The function possessing orthorhombic symmetry consists of eight equal “petals,” which have maxima at angles $(\beta_{\max}, \gamma_{\max})$, $(\beta_{\max}, -\gamma_{\max})$, $(\beta_{\max}, \pi + \gamma_{\max})$, $(\beta_{\max}, \pi - \gamma_{\max})$, $(\pi - \beta_{\max}, \gamma_{\max})$, $(\pi - \beta_{\max}, -\gamma_{\max})$, $(\pi - \beta_{\max}, \pi + \gamma_{\max})$, $(\pi - \beta_{\max}, \pi - \gamma_{\max})$. For the function presented in Figure 17(a), β_{\max} is approximately 90° , as the petals corresponding to the angles $(\beta_{\max}, \gamma_{\max})$ and $(\pi - \beta_{\max}, \gamma_{\max})$, $(\beta_{\max}, -\gamma_{\max})$ and $(\pi - \beta_{\max}, -\gamma_{\max})$, etc. overlap in pairs.

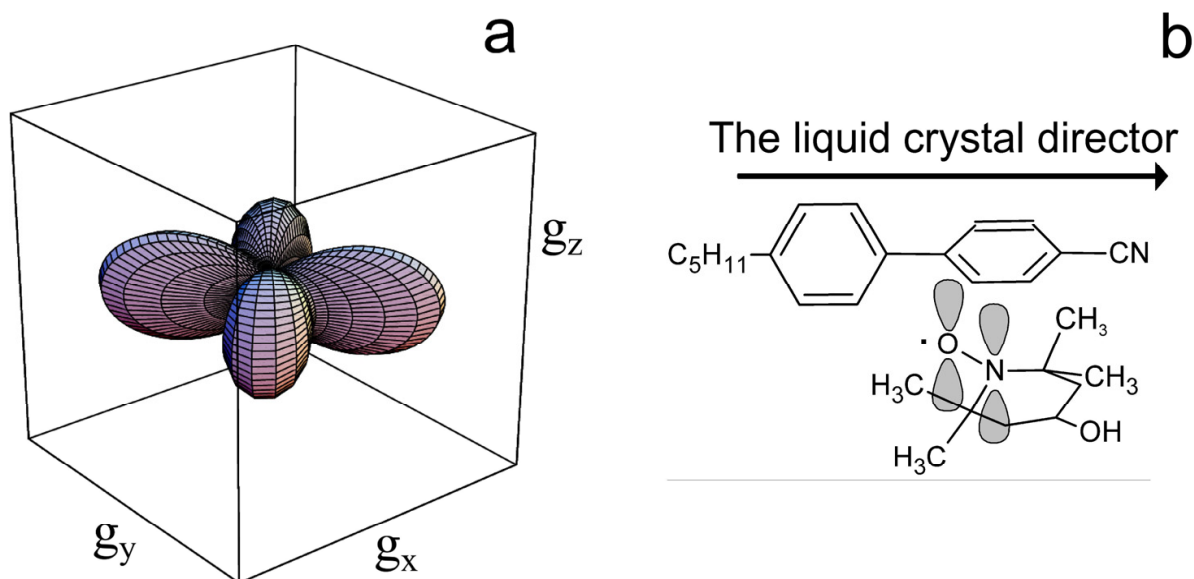


Figure 17. The orientation distribution function of TEMPOL in 5CB aligned by the magnetic field (a) and the reciprocal orientation of the molecules of the spin probe and liquid crystal (b).

In Figure 18, one can see the angular dependence of the EPR spectrum for the nitroxide radical $V(n = 11)$ in supercooled 5CB aligned by magnetic field and the result of the computer simulation of spectra [76]. It is seen that angular dependence (the difference between the spectra recorded at different angles) in the case of the spin probe $V(n = 11)$ is much larger than in the case of TEMPOL. Obviously, molecules of probe V , which have rigid central fragments, are built into a liquid crystal structure better than the molecules of TEMPOL. It was found out that orientation function in this case is determined reliably up to the sixth order of expansion. The values of the coefficients are presented in Table 5. The function is shown in Figure 19. It can be seen that the central rigid fragments of the paramagnetic molecules preferably order along the liquid crystal molecules. The magnetic axis X is situated perpendicular to the sample director.

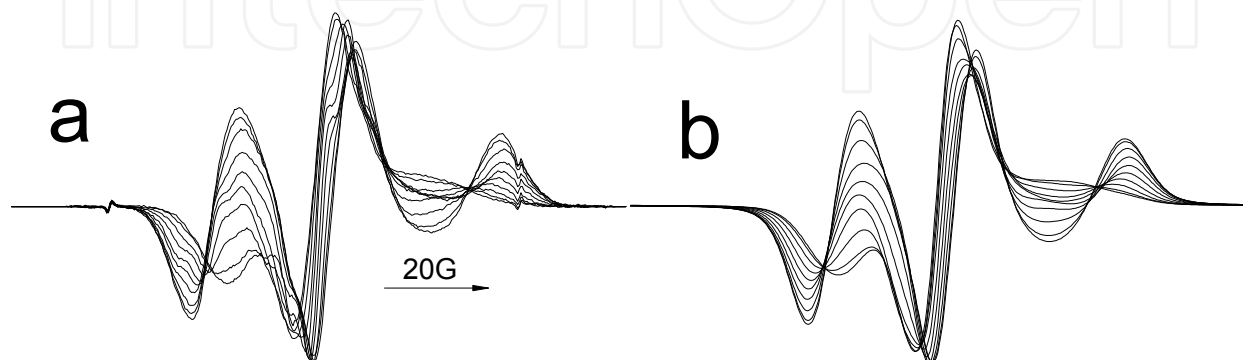


Figure 18. The angular dependence of the EPR spectrum of the nitroxide radical $V(n = 11)$ in 5CB aligned by magnetic field (a) and the result of its computer simulation (b).

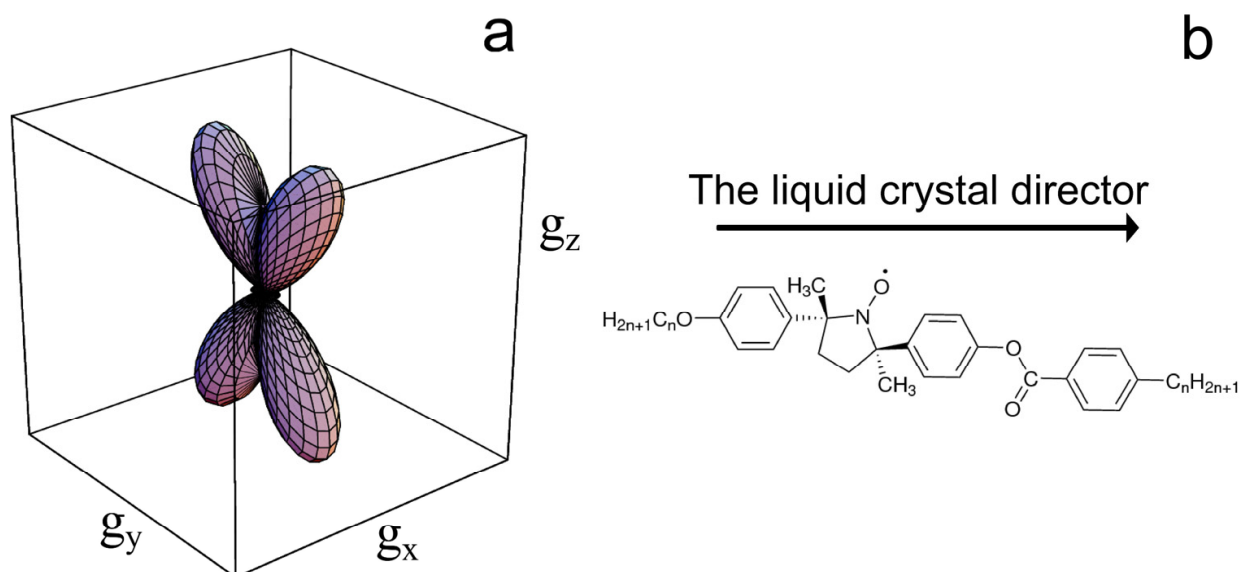


Figure 19. The orientation distribution function of radical $V(n = 11)$ in 5CB aligned by the magnetic field (a) and orientation of the molecules of spin probe and liquid crystal (b).

In the examples presented earlier, the uniaxial samples were studied. However, the method described can be used for investigating more complicated systems. In Figure 20, one can see the scheme of the following experiment. The sample of liquid crystal 5CB with embedded the spin probe TEMPOL was aligned by the magnetic field of the EPR spectrometer along the direction D_1 at $T = 295\text{K}$ and then was quickly cooled to $T = 77\text{K}$ as it was performed in the previous examples. After that, the sample was heated in the spectrometer resonator to $T = 220\text{K}$ in such position that the axis D_1 was approximately perpendicular to the magnetic field direction. In the course of this annealing, the new axis D_2 directed along the new magnetic field vector arose. After realignment, the sample was quickly cooled in the magnetic field to $T = 77\text{K}$, and the angular dependence of EPR spectra was recorded. The orientation distribution for this sample was presented as a sum of two different uniaxial functions with different directors, D_1 and D_2 . The varied parameters in this case were the expansion coefficients of these functions in series (15) and the fractions of particles oriented along the D_1 and D_2 axes. In this assumption, it was possible to simulate the angular dependence of the EPR spectrum within the experimental errors. The orientation distributions of the probe molecules respective to D_1 and D_2 axes are shown in Figure 20 (functions F1 and F2, correspondingly). One can see that the function F1 is practically equal to the function presented in Figure 17(a). Hence, a part of the liquid crystal is not realigned by magnetic field at $T = 220\text{K}$. Another part of the sample possesses mobility at $T = 220\text{K}$, which is sufficient to change the orientation according to the new director D_2 ; thus, this part of the probe molecules are turned at an angle of 90° . One can see that the mobility of the liquid crystal particles at $T = 220\text{K}$ is sufficient for realization of realignment. The ratio of the number of radicals oriented axially along D_1 to those oriented axially along D_2 is 2.5:1. As a whole, the result of this experiment provide evidence of considerable distribution of molecular mobility in supercooled liquid crystal.

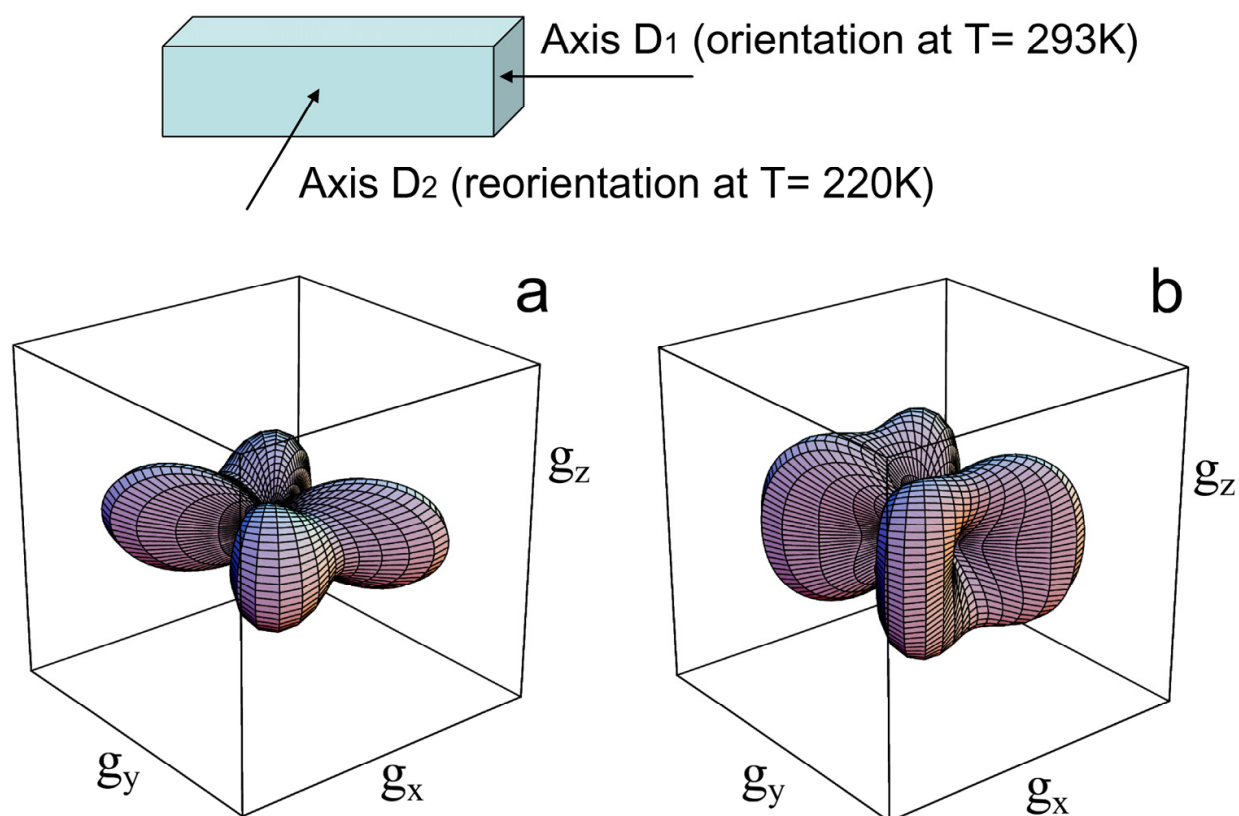


Figure 20. The scheme of the experiment of the liquid crystal realignment (see text). The distribution functions for axis D_1 (a) and axis D_2 (b) in the molecular reference frame.

4.3. Non-orthorhombic spin probe

In all the previous examples, nitroxides were used as spin probes. For these radicals, the directions of the main axes of the g - and hfi -tensors coincide, and the orientation distribution possesses orthorhombic symmetry. In series (15) in this case, only coefficients a_{jm} with even j and m are nonzero. This feature is a consequence of the existence of eight molecular orientations undistinguishable by EPR. To characterize molecular order more definitely, the paramagnetic probe with lower symmetry is necessary. In the following text, we present an example of orientation distribution of HO_2 radicals with distinct axes of g - and hfi -tensors [77]. The HO_2 -radicals were generated in the matrix of glassy hydrogen peroxide at 77K by the light irradiation with wavelength $\lambda = 254$ nm. The long irradiation by the collimated beam of the nonpolarized light leads to orientational alignment of the radicals as a result of the photo-orientation process. In the course of photo orientation, the radicals are aligned in such a way that the vectors of their optical dipole transition moments are directed along the symmetry axis of the sample (direction of light beam). By means of simulation of the spectrum of the isotropic sample, it was established that the Euler angles connecting the frames of the g - and hfi -tensors come to $\zeta = -70^\circ$, $\xi = 47^\circ$, and $\varsigma = 35^\circ$. Hence,

in this case, the magnetic properties of paramagnetic particles cannot be described by tensor rank two, and each direction in the radical coordinate frame is individual and can be found from the analysis of the EPR spectra. Series (15) in this case includes nonzero coefficients a_{jm} и b_{jm} with both even and odd m . The orientation distribution function of the HO₂-radicals is presented in Figure 21; the expansion coefficients are shown in Table 5. One can see that in this case, one predominant orientation of the radicals respective to the sample symmetry axis is observed. Obviously, this orientation is dictated by the optical dipole transition moment of HO₂. Hence, determination of the orientation distribution function of the paramagnetic molecules allows establishing experimentally the direction of optical dipole transition moment in the molecular coordinate frame.

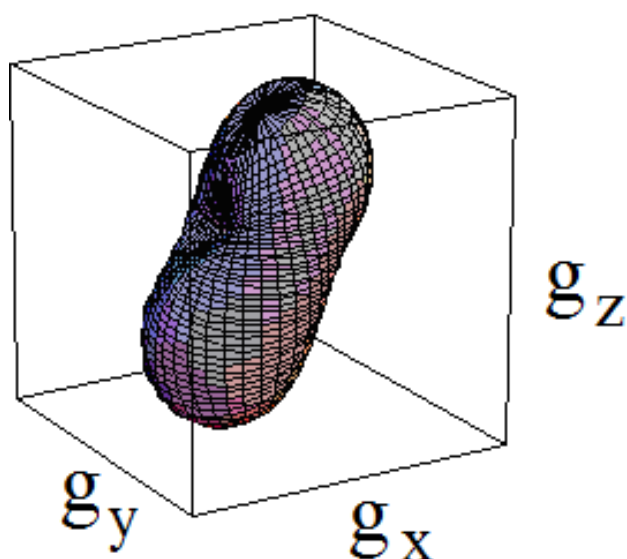


Figure 21. The orientation distribution function of the HO₂-radicals in supercooled hydrogen peroxide.

4.4. Molecular orientation frame

In the example presented previously, the data concerning the properties of the paramagnetic molecules were obtained. However, most often, orientation distribution of the spin probe is studied to obtain information about the structure and dynamics of the matrix. In this case, the choice of the spin probe is of fundamental importance. It was shown earlier that radical V reflect the alignment of liquid crystals more effectively than the standard spin probes of the piperidine series. As another illustration of the sensitivity of the method to the structure of the probe, the orientation distributions for different radicals in the thin film of polyethylene stretched by five times are shown in Figure 22. It is seen that radicals that have rigid central fragment $V(n = 4)$, $V(n = 11)$, and $V(n = 15)$ are ordered in this matrix more effectively than the imidazolidine derivative VI (Figure 3). At the same time, ordering of radical V depends on the length of the saturated substituents, which evidently align in the polymer matrix along the macromolecules of polyethylene.

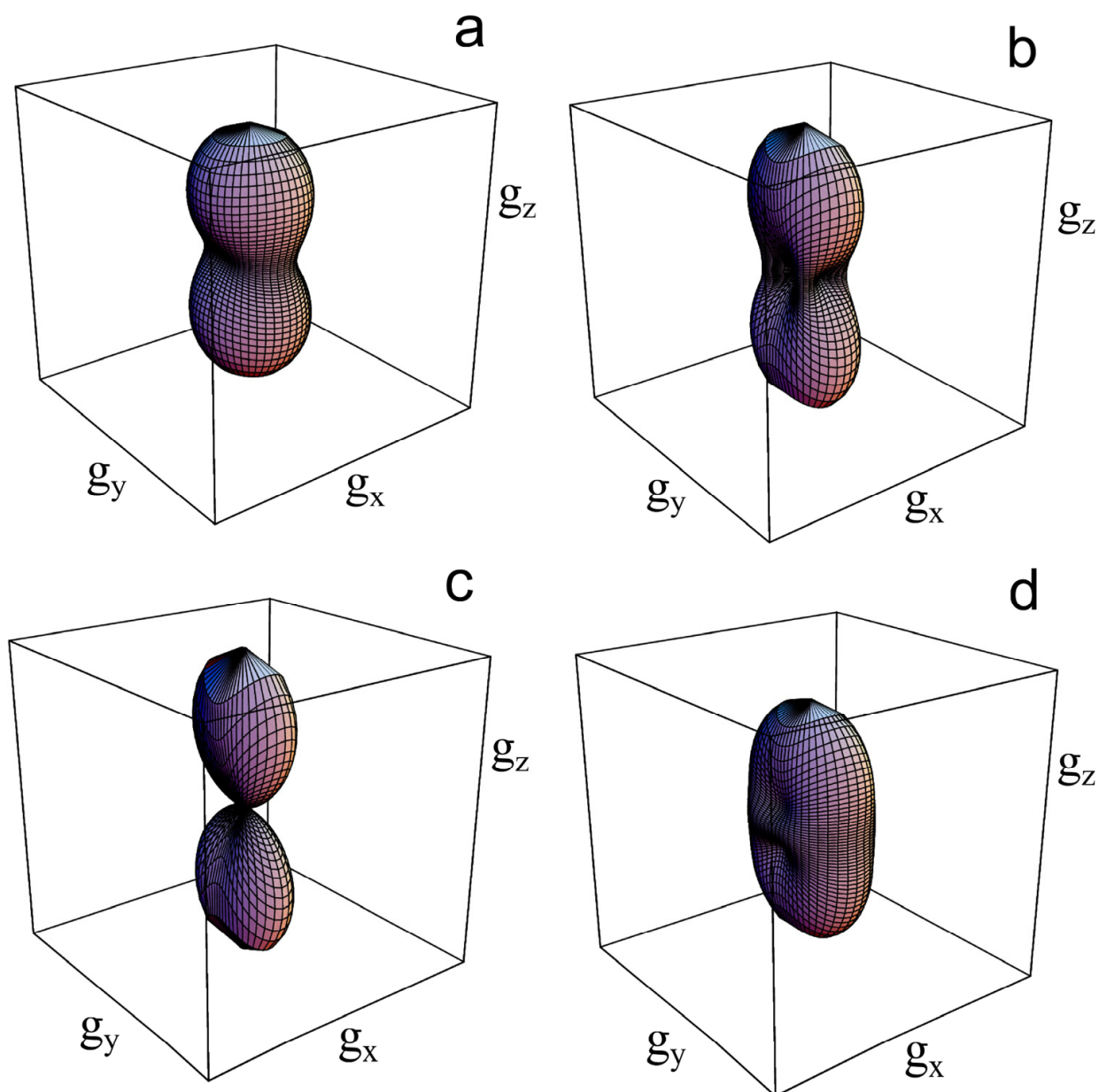


Figure 22. The orientation distribution function of the radicals $V(n = 4)$ (a), $V(n = 11)$ (b), $V(n = 15)$ (c), and VI (d) in the polyethylene film stretched five times.

It is obvious that orientation of a paramagnetic molecule in the ordered matrix is defined not by magnetic axes but by other molecular properties (geometric shape, interaction with the medium molecules, etc.). In every case, there is a molecular axis that is ordered to the maximum extent. This axis will be referred to as main molecular orientation axis Z_t . The second most ordered axis, which is orthogonal to the first one, defines completely the molecular orientation frame (X_t , Y_t , Z_t). A practically important problem is to establish the direction of the orientation axes of the paramagnetic molecules relatively to known axes, for example, principal g -tensor axes. In addition, it is necessary to determine the order parameters (orientation factors) for the orientation axes because such parameters more adequately reflect orientation alignment of media.

As it was noted previously, uniaxial samples are studied commonly in practice. At the same time, most spin probes have three different principal values of g-tensor. The formation of the uniaxial sample by orthorhombic particles can be done in two ways, which are illustrated in Figure 23. First, such situation can be realized if all three orientation axes are ordered axially in the sample (they form the cones around the symmetry axis of the sample; Figure 23a). Let us call this type of the uniaxial sample A1. The second possibility is shown in Figure 23b. In this case, one orientation axis (denote it as Z_t) is ordered axially in the sample (forms the cones around the symmetry axis) and two other orientation axes are directed statistically in the plane ($X_t Y_t$). In this type of axial sample (A2), we will name the case of hidden molecular axiality.

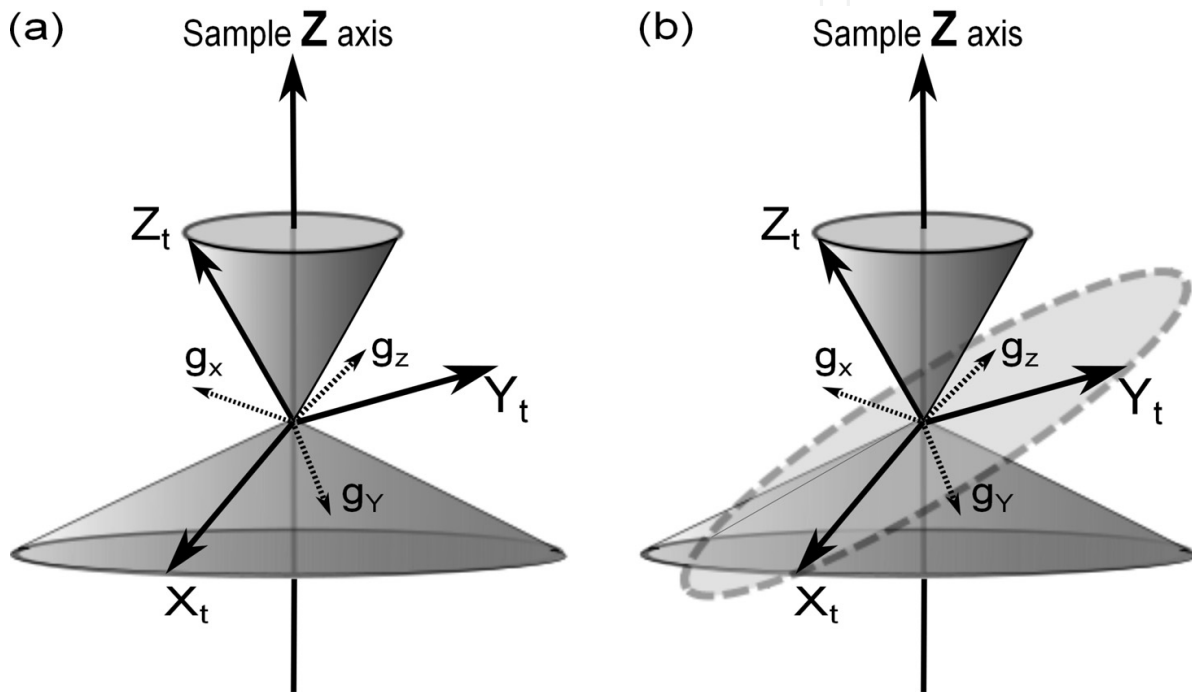


Figure 23. Mutual disposition of the magnetic and orientation frames of the spin probe and the sample director: A1 (a) and A2 (b) (see text).

It can be shown that the expansion coefficients of the distribution function presented in the molecular orientation frame and the coefficients for the same function described in the g-tensor frame in the case of the A1 sample are connected by the following expression:

$$\langle D_{m'm}^j \rangle_{gF} = \sum_k \langle D_{m'k}^j \rangle_t D_{mk}^j(\varphi, \theta, \psi), \quad (19)$$

where angles φ , θ , and ψ are Euler angles connecting the molecular orientation frame with the g-tensor frame.

Orientation distribution function of the sample symmetry axis in the molecular orientation frame of the spin probe has a maximum along the axis Z_t . In the case of A2, this function possesses uniaxial symmetry and can be described by series (15), in which only members with zero second indices are nonzero:

$$\rho(\beta_t) = \frac{1}{4\pi} \sum_{j=0}^{\infty} (a_{j0})_t P_j(\cos \beta_t) \quad (20)$$

where β_t is the angle between the symmetry axis of the sample and the axis Z_t and $(a_{j0})_t$ are the expansion coefficients in series (15) for the distribution function presented in the molecular orientation frame (X_t, Y_t, Z_t).

Let the angles (θ, φ) determine the direction of Z_t in the g-tensor frame. Using Eq. (19), it can be shown that the expansion coefficients of the function in the g-frame $(a_{j0})_{gF}$ are connected with the coefficients $(a_{j0})_t$ and angles (θ, φ) by the following expression:

$$\begin{aligned} \langle D_{0m}^j \rangle_{gF}^* &= (A_0^j)_t D_{m0}^j(\varphi, \theta, 0) \\ a_{jm} &= (a_{j0})_t \frac{(-1)^m (j-m)!}{(j+m)!} \cos m\varphi P_{jm}(\cos \theta) \\ b_{jm} &= -(a_{j0})_t \frac{(-1)^m (j-m)!}{(j+m)!} \sin m\varphi P_{jm}(\cos \theta) \end{aligned} \quad (21)$$

Using Eq. (21) in the course of the computer simulation of the spectrum angular dependence, one can vary coefficients $(a_{j0})_t$ and angles (θ, φ) and simultaneously find the order parameters and direction of the main molecular orientation axis in the g-tensor frame of the radical. It is necessary to note that in the case of orthorhombic probe, one of the eight undistinguishable pairs (θ, φ) is determined in the course of such calculations.

In the case A1, the orientation distribution function described in the molecular orientation frame does not possess uniaxial symmetry and can be described by angles (φ, θ, ψ) and coefficients $(a_{jm})_t$, including the members with nonzero m in accordance with Eq. (19).

The possibilities of simulation of the spectrum angular dependence according to assumptions A1 and A2 are contained in the program ODF3.

In Figure 24, one can see the orientation functions of the radical $V(n = 11)$ in supercooled 5CB aligned by magnetic field of the EPR spectrometer. The function in Figure 24(a) was obtained in orthorhombic assumption; the function in Figure 24(b) corresponds to hidden axiality **A2**. It is seen that Eq. (21) permit to separate one petal from orthorhombic function. The discrepancy of the calculated spectra from the experimental ones for these two functions is the same. This calculation leads to the determination of the main molecular orientation axis for the probe V. This axis was found to be directed with the angles $\theta = 30^\circ$, $\varphi = 0^\circ$ to the g-tensor axes. It was verified that the other seven pairs of angles mentioned earlier lead to the same calculated spectra. Hence, the choice between these possible directions can be done only by using additional data obtained by other experimental techniques.

The analogous functions are presented in Figure 25(a, b), but in this case, the liquid crystal was aligned in uniaxially ordered cylindrical pores of porous polyethylene [78]. Figures

24(b) and 25(b) show that the obtained functions are very close. The difference between the functions consists in the extent of anisotropy. It is seen that liquid crystal 5CB is aligned by magnetic field more effectively than by the pores of polyethylene. The significant visual difference between the orthorhombic functions 24(a) and 25(a) is explained by the fact that individual petals that are well divided in function 24(a) become wider and flow together in function 25(a).

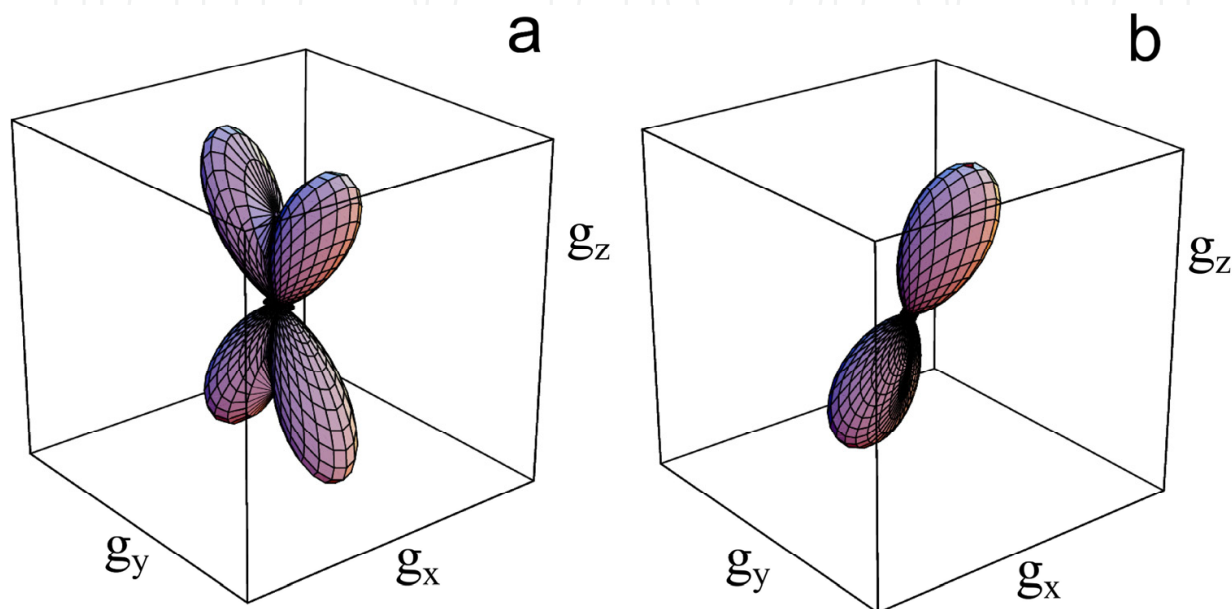


Figure 24. The orientation distribution functions of radical $V(n = 11)$ in 5CB aligned by the magnetic field: the orthorhombic function (a) and the function calculated with the assumption A2 (b).

Almost all the cases presented previously showed that the simulations within the uniaxial models A1 and A2 lead to the very close values of discrepancy between the calculated and experimental spectra. It means that the model of hidden axiality is often confirmed by experiment. The exception was found in the case of liquid crystal aligned in porous polyethylene. In that case, the simulation of the angular dependence for $V(n = 11)$ in the assumption A1 leads to diminishing of discrepancy by 14% in comparison with the model A2. The found distortion of uniaxial symmetry of the distribution is shown in Figure 25(c, d). This example demonstrates that the biaxiality of nematic media can be studied by spin probe technique.

4.5. Order parameters

On the basis of orientation distribution function, one can calculate the order parameters for any molecular axis of the radical in the matrix under consideration. For this aim, orientation distribution functions are transformed to the chosen molecular frame using Eq. (19) or (21). The order parameters for new axes are calculated according to Eq. (16).

The second-rank order parameters for the g -tensor axes can be calculated as follows:

$$A_0^2(g_x) = -\frac{a_{20}}{10} + \frac{6a_{22}}{5} \quad (22)$$

$$A_0^2(g_y) = -\frac{a_{20}}{10} - \frac{6a_{22}}{5} \quad (23)$$

$$A_0^2(g_z) = \frac{a_{20}}{5}, \quad (24)$$

where a_{20} and a_{22} are obtained in orthorhombic approximation in the g-tensor frame.

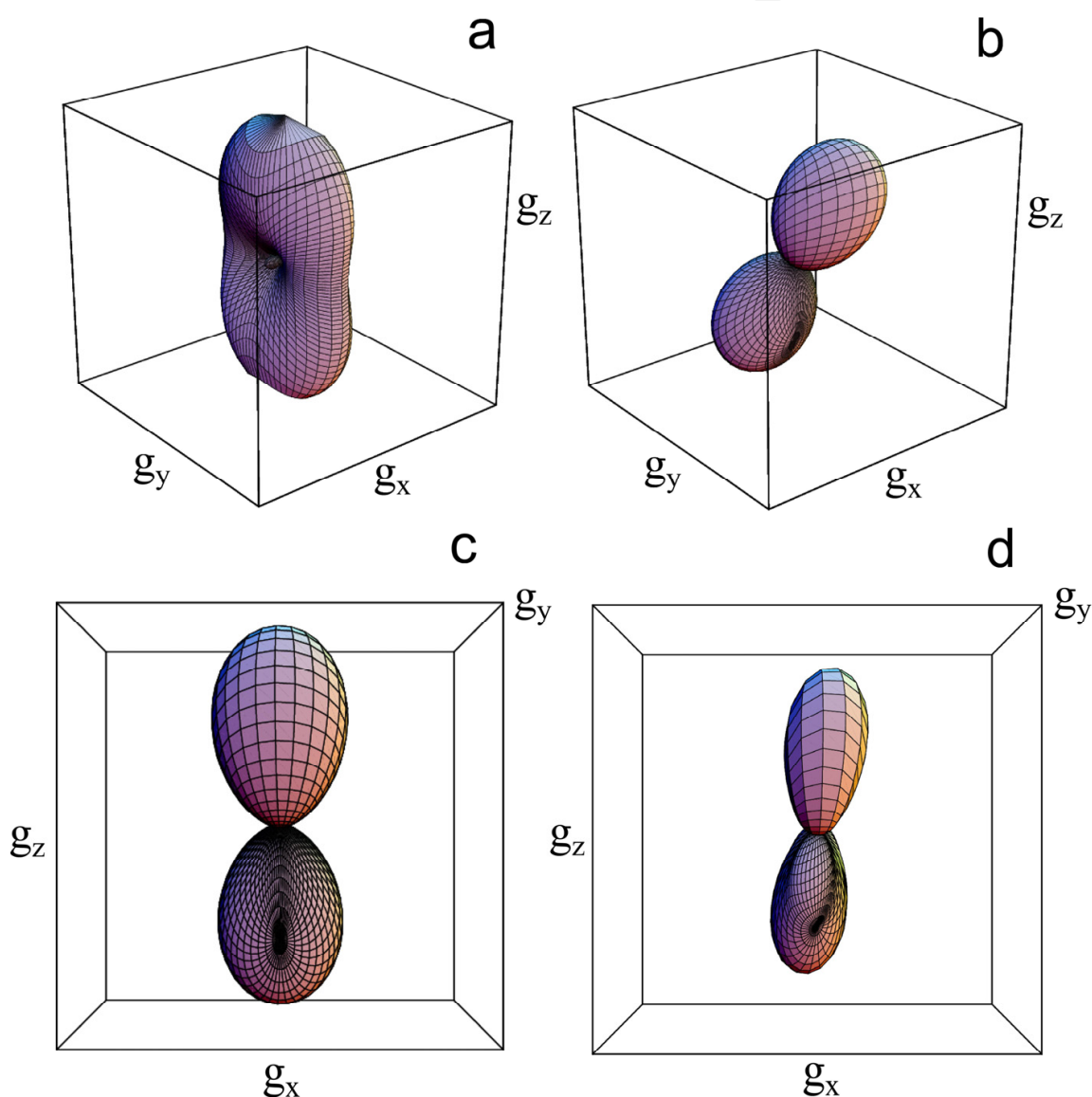


Figure 25. The orientation distribution functions of radical $V(n = 11)$ in 5CB aligned in the pores of the porous polyethylene: orthorhombic function (a), the function calculated with the assumption A2 (b,c), and function calculated with the assumption A1 (d).

The order parameters for the magnetic axes of the radical $V(n = 11)$ in 5CB aligned by magnetic field (Figure 24(a)) arrive at the values $f(g_x) = -0.35$, $f(g_y) = -0.031$, and $f(g_z) = 0.38$. These values show that the axis X is ordered predominantly perpendicular to the symmetry axis of the sample. The order parameters for axes Y and Z are determined not only by their extent of ordering but also by the angles between these axes and the director of the sample. Rather small values of the order parameters for the magnetic Y and Z axes reflect the tilt of these axes relative to sample director. Thus, the values of the order parameters for magnetic axes are useful in defining the orientation of the probe relative to the medium but do not characterize clearly the medium alignment.

The more adequate characteristics of the medium order are the order parameters of the probe orientation axes. The values calculated using Eqs. (21) and (16) for some studied liquid crystalline systems are collected in Table 6. One can see from the table that the second-rank order parameters achieve the values 0.6–0.7, which are in agreement with the values for nematic mesophase obtained by other methods. The important advantage of the presented method is the possibility to estimate order parameters of higher rank. Some of these values are presented in Table 6 as well.

Systems	$(A_{20})_t$	$(A_{40})_t$	$(A_{60})_t$
$V(n=11)$ in 5CB	0.626	0.347	0.148
$V(n=15)$ in stretched PE	0.673	0.357	0.088
$V(n=11)$ in 5CB/pores	0.522	0.089	–
I-trans in 5CB/pores	0.376	0.059	–
I-cis in 5CB/pores	0.206	0.013	–
Errors	~3%	~12%	~15%

Table 6. Order parameters obtained within the assumption of A2 axially

At present, the most widespread technique for the study of orientational alignment is optical spectroscopy, particularly the measuring of the linear dichroism in UV-vis range. It is known that such measurements give only order parameters of rank 2 [79]. To verify the discussed EPR technique, it is important to compare the values obtained by EPR and the optical measurements for the same samples. Such comparison is presented in Table 7 using four systems.

The orientation distribution of anion-radicals Cl_2^- in low temperature glass formed by 5M aqueous solution LiCl at 77K is studied in [80]. The orientational alignment in this system was induced by irradiation of the sample with parallel beam of the linearly polarized light using photo-orientation phenomenon. In this case, the anion-radicals are predominantly oriented perpendicular to the electric vector of light wave. Taking into account that optical transition moment directed along the axis of anion-radical, the order parameter of rank two can be measured as linear dichroism:

$$A_{0opt}^2 = d = \frac{D_{\parallel} - D_{\perp}}{D_{\parallel} + 2D_{\perp}}, \quad (25)$$

where D_{\parallel} and D_{\perp} are the values of optical absorbance at mutually parallel and perpendicular polarizations of the irradiating and probing beams. The dichroism of the sample presented in the table was averaged over the range of wavelengths from 349 to 390 nm.

	Anion-radical Cl_2^- in glassy aqueous solution of LiCl	<i>Trans</i> -I in 5CB embedded in pores of polyethylene	<i>Cis</i> -I in 5CB embedded in pores of polyethylene	$V(n = 4)$ in liquid crystalline comblike polymer
A_{0EPR}^2	-0.10 ± 0.01	0.38 ± 0.01	0.21 ± 0.01	$0.55 \pm 0.03^*$
A_{0opt}^2	-0.12 ± 0.01	0.35 ± 0.04	0.23 ± 0.03	$0.36 \pm 0.01^{**}$

*Orientation factor of the orientation axis of radical $V(n = 4)$

**Orientation factor of the optical transition dipole moment of merocyanine dye (Figure 26)

Table 7. The order parameters determined by means of optical spectroscopy and EPR

The dichroism of the samples containing the ordered radical I in *cis* and *trans* forms was measured similarly using the recording of UV-vis spectra in polarized light. The radicals were ordered in 5CB aligned in pores of polyethylene.

To obtain the order parameters for ordered comblike liquid crystalline polymer (Figure 26) by means of EPR spectroscopy, the spin probe $V(n = 4)$ was used. For measurements of linear dichroism, merocyanine dye Ash253a was embedded in the sample.

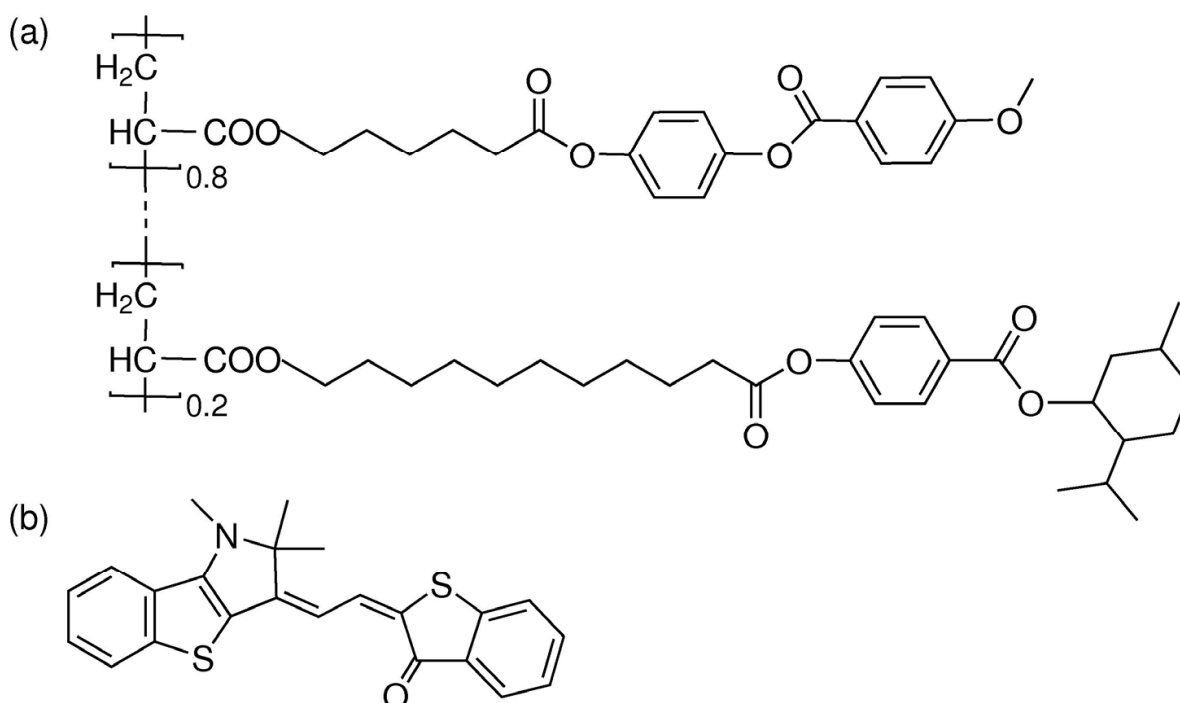


Figure 26. The structures of comblike polymer containing racemic menthyl moieties and nematogenic phenylbenzoate moieties (a) and merocyanine dye Ash253a (b).

One can see from Table 7 that the EPR technique produces the values of the order parameters, which are in agreement with the optical measurements. The noticeable difference is observed only in the case of comblike polymer when the dichroism of specially introduced dye was measured. Possibly, the optical measurement in this case gives the understated value as a result of the tilt of the transition dipole moment with respect to the director of liquid crystal matrix. Thus, the proposed method is efficient for determining order parameter.

4.6. Determination of orientation distribution function of rotating radicals

The serious disadvantage of the method described previously is the impossibility of using the EPR spectra if probe molecules rotate in the time scale of EPR. Many systems of great interest can exist only in temperature ranges in which the intensive molecular rotational mobility takes place. Orientational alignment of the nematic phases presented previously was studied by means of quick cooling of the samples to $T = 77\text{K}$ and subsequent recording of the spectra of fixed particles. We supposed that the structure of the material does not change considerably at such cooling. However, such an approach cannot always be used. For example, the temperature dependence of the liquid crystal structure or alignment cannot be studied using this approach.

At present, the most widespread method for simulation of EPR spectra of rotating spin probes with determination of orientation distribution function is the method described in [4, 5]. This method is based on the assumption that each paramagnetic molecule is situated in the field of ordering potential, which is induced by the aligned matrix $U(\alpha, \beta, \gamma)$. This approach will be referred henceforth as ordering potential (OP) method to distinguish from the method described earlier, the orientation function (OF) method. The orientation distribution of the molecules in the potential is determined by the Boltzmann equilibrium:

$$\rho(\beta, \gamma) = \frac{e^{-U(\beta, \gamma)/k_b T}}{\int e^{-U(\beta, \gamma)/k_b T} \sin \beta d\beta d\gamma} \quad (26)$$

The ordering potential is represented as a series of spherical functions:

$$\frac{U(\beta, \gamma)}{k_b T} = -\sum_{j, m} c_{jm} D_{0m}^j(\beta, \gamma) \quad (27)$$

In practice, the expression (24) is presented as follows:

$$\frac{U(\beta, \gamma)}{k_b T} = -\sum_j c_{j0} D_{00}^j(\beta, \gamma) - \sum_{j, m} c_{jm} [D_{0m}^j(\beta, \gamma) + D_{0-m}^j(\beta, \gamma)], \quad (28)$$

where $j, m = 2, 4$.

The program realization of the OP method is based on the stochastic Liouville equation; hence, it can be used for analysis of the orientation ordering of the rotating molecules. The

available software for the OP method utilizes the assumption that the axis of fastest rotation of the paramagnetic molecule is directed along the orienting potential. A lot of useful and important information concerning different oriented media was obtained using this method [6-11].

For comparison of the results obtained by the OP and OF methods, we determined the orientation distribution functions of some spin probes in the liquid crystal 5CB, aligned in pores of the porous polyethylene, at the temperature of liquid nitrogen, $T = 77\text{K}$ (OF), and at the temperature of existence of the nematic phase, $T = 298\text{K}$ (OP). It was found that 5CB ordered in the pores is not affected by the orienting action of the magnetic field of the EPR spectrometer. Therefore, it is possible to record the angular dependence of the EPR spectrum of such sample at $T = 298\text{K}$.

In Figure 27(b), one can see the orientation distribution function determined by the OP method at $T = 298\text{K}$. Visually, this function is quite identical to the function obtained for the same system by means of the OF method at $T = 77\text{K}$ (Figure 27(a)). The order parameter of the axis of the fastest rotation of the paramagnetic molecule in this case comes to $(A_0^2)_{\text{rot}} = 0.48$ and agrees within the experimental errors, with the value of the order parameter obtained by means of the OF method, $(A_0^2)_t = 0.50$. The direction of the rotation axis in the magnetic frame is described by the angles $\theta_{\text{rot}} = 39^\circ$ and $\varphi_{\text{rot}} = 0^\circ$; it is close to the direction of the orientation axis $\theta_t = 30^\circ$, $\varphi_t = 0^\circ$. Evidently, the molecular orientation axis in this case coincides with the axis of the fastest rotation, and the methods OP and OF give the same results. This example shows as well that the structure of the matrix really does not noticeably change at rapid cooling of the sample by immersing it into liquid nitrogen.

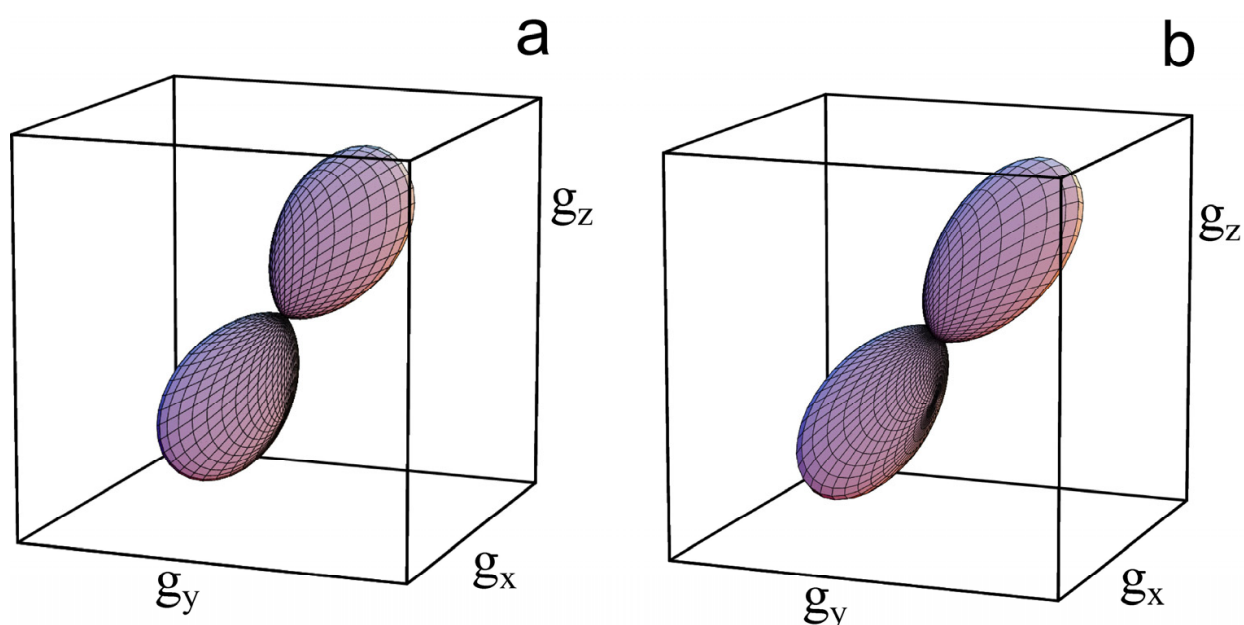


Figure 27. The orientation distribution function of radical $V(n=11)$ in 5CB defined from the room temperature spectra by the OP method.

The similar comparison of the methods OP and OF was performed by determination of the orientation functions of the nitroxide radicals containing azobenzene fragment (Figure 28) in 5CB aligned in the pores of polyethylene. Conversion of the azobenzene moiety from *trans* to *cis* form was realized by irradiation of the samples with light [62].

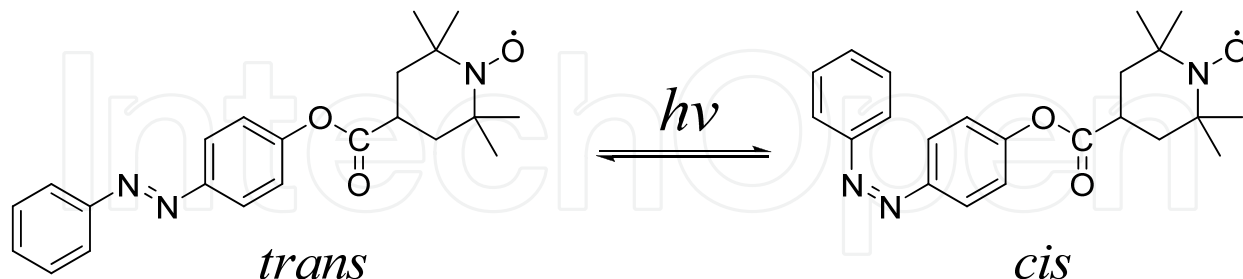


Figure 28. Photochemical conversion of the azobenzene fragment of radical I.

In Figures 29 and 30, one can see the orientation distribution functions of radical I in *trans* and *cis* configurations. The functions were determined at temperatures $T = 77\text{K}$ (OF method; Figures 29(a) and 30(a)) and $T = 298\text{K}$ (OP method; Figures 29(b) and 30(b)). The obtained characteristics are collected in Table 8.

System	$(a_{20})_t, (a_{40})_t$	θ_t, φ_t , degree	$(A_{0^2})_t$	$c_{20},$ c_{22}	$c_{40},$ $c_{40},$ c_{40}	$\theta_{rot}, \varphi_{rot}$, degree	$(A_{0^2})_{rot}$
V(n=11) in 5CB/pores	2.61 ± 0.02 0.80 ± 0.08	$33.6 \pm 0.2,$ 90.3 ± 1.4	0.52	2.22 ± 0.15 0.32 ± 0.05	–	40.7 ± 0.4 109.3 ± 1.0	0.48
I- <i>trans</i> in 5CB/pores	1.88 ± 0.02 0.53 ± 0.03	86.8 ± 2.2 11.9 ± 0.7	0.38	1.24 ± 0.01 -0.080 ± 0.002	–	106.4 ± 0.2 10.2 ± 0.3	0.28
I- <i>cis</i> in 5CB/pores	1.03 ± 0.02 0.17 ± 0.02	86.1 ± 2.8 -42.4 ± 0.3	0.21	0.23 ± 0.01 -0.121 ± 0.001	0.22 ± 0.01 0.17 ± 0.01 0.26 ± 0.01	90.0 ± 1.2 5.4 ± 0.08	0.05

Table 8. Parameters of the orientation distribution functions defined by the OP and OF methods

It is seen that in the case of the probe in *trans* form, the direction of the main rotational axis ($\theta_{rot} = 10^\circ, \varphi_{rot} = 106^\circ$) does not coincide with the direction of the molecular orientation axis ($\theta_t = 12^\circ, \varphi_t = 87^\circ$), although the deviation is not large. The order parameter value determined by the OP method is noticeably lower than value obtained by the OF method (0.28 and 0.38, correspondingly). This disagreement becomes dramatic in the case of the probe in *cis* configuration. This comparison demonstrates that the OP method produces understated and unreliable data when the molecular orientation axis of the probe does not coincide with the main rotation axis.

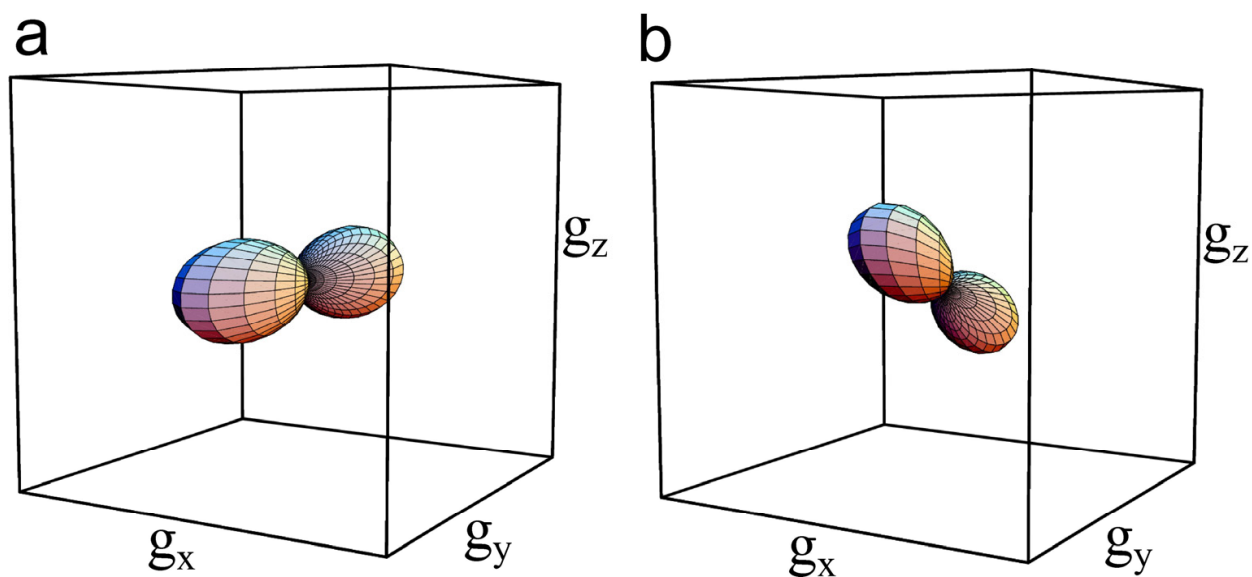


Figure 29. The orientation distribution functions of radical I in *trans* configuration defined by the OF (a) and OP methods (b).

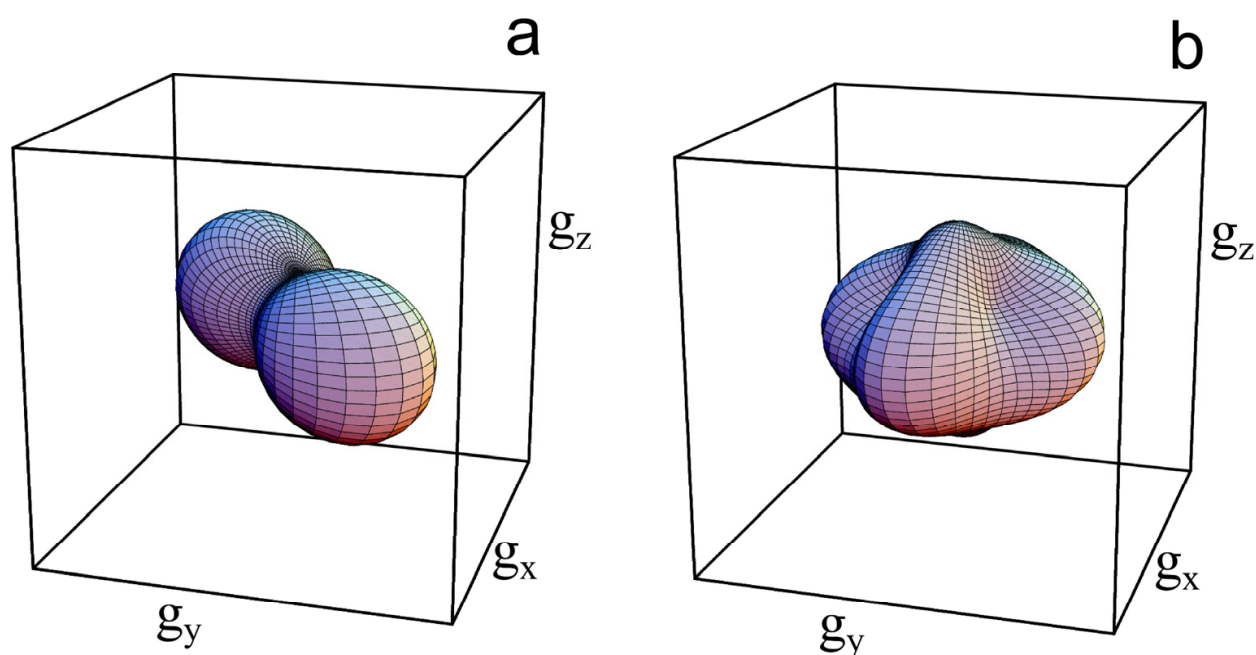


Figure 30. The orientation distribution functions of radical I in *cis* configuration defined by the OF (a) and OP methods (b).

Unfortunately, the OP method has some other disadvantages. One of them is the assumption of Boltzmann distribution of the particles in the field of oriented potential. Boltzmann law is fulfilled locally in most cases. However, each probe molecule is in the surrounding that differs from the surrounding of other molecules by direction and magnitude of potential. As a result, the orientation distribution function as a whole, in general case, cannot be described by simple Boltzmann formula. This drawback becomes a serious obstacle to the application of the model when the local directors in liquid crystal do not coincide with the sample director, for example, when the clear domain structure or

cholesteric order exists in the medium. The OP method can be applied for analysis of polydomain samples only in the case of statistical (chaotic) orientation of the domains. Such approach is called microscopic order–macroscopic disorder (MOMD).

The most essential weakness of the OP method is the interdependence of determined parameters. The coefficients of rotation diffusion and the characteristics of ordering potential are not independent when single EPR spectrum is treated. As a result, few different optimal set of parameters produce almost the same calculated spectra. Hence, it is impossible to determine unambiguously the rotation diffusion coefficients and orientation parameters by means of simulation of a single EPR spectrum. This problem is solved to some extent by simultaneous simulation of a series of spectra recorded at various orientations of the sample in the magnetic field. However, such experiment cannot always be performed. For example, recording of the spectrum angular dependence of spin probes in a nematic liquid crystal at the temperature of mesophase is impossible, as the nematic phase is oriented by the magnetic field of the spectrometer. In such case, to record the angular dependence, it is necessary to undertake additional efforts: to align the sample by electric field, to put liquid crystal into the polymer pores, etc. The mutual correlation of different coefficients c_{jm} , which characterize the ordering potential, prevents the reliable determination of the order parameters with a rank more than two even when the set of spectra with different sample orientation is simulated.

5. Conclusions

The data presented in this chapter lead to the following conclusions. Owing to the modern computing technique that allows simultaneous simulation of the set of EPR spectra, some methods for extraction of the quantitative information from the spectra were developed. These methods broaden significantly the area of application of the spin probe technique and make it possible to investigate subtle features of the structure and molecular dynamics of various materials. On the other hand, it is clear that possibilities opened are not used quite effectively.

First of all, it is necessary to note that at present, there is no method for reliable distinction of the influences of rotation and orientation of the radicals on the shape of EPR spectra. One more problem that is close to solution by means of the spin probe method is the determination of the high-rank order parameters. There is no theoretical prohibition for determination of these parameters by the EPR method. However, the existing approach based on the ordering potential is unable to provide reliable values of high-rank order parameters. The direct expansion of the orientation function in a series of generalized spherical harmonics (a model-free technique) overcomes this drawback but is unable to use the spectra recorded at high molecular mobility. One more basic problem in the field is the elaboration of the accurate mathematical criteria for calculation of errors that appear in the course of solving the inverse problem during the spectra simulation.

In our opinion, insufficient attention is paid to consideration of the concentration broadening of the EPR spectra. Whereas the simulation of the exchange-broadened spectra

is possible in the program package [4], the description of the spectral line broadening in the case of dipole-dipole interaction of radicals and, moreover, in the cases of dipole-dipole and exchange interactions is impossible. Elaboration of appropriate methods would be useful for determination by means of spin probe technique of not only orientational but also translational order of liquid crystal materials, biological membranes, and films. In such case, one could see the whole spectrum of intermediate states appearing during formation of one or another ordered phase.

We hope that the methods presented in this chapter and the proposed open-code computer programs will serve to develop more complete methods of analysis of the EPR spectra of spin probes.

Author details

Andrey Kh. Vorobiev and Natalia A. Chumakova
Department of Chemistry, M.V. Lomonosov Moscow State University, Leninskie Gory, Moscow, Russia

Acknowledgement

The authors acknowledge the financial support of the Russian Foundation for Basic Research (grant no. 09-03-00900-a). The authors thank Prof. S. Nakatsuji (University of Hyogo) and Prof. R. Tamura (Kyoto University) for the provision of paramagnetic probes and Prof. G. K. Elyashevitch for the provision of stretched porous polyethylene films.

Appendix

Program ODF3

The program ODF3 is elaborated for simulation of the EPR spectra and determination of the spectra parameters by the fitting procedure. The program is a working tool used in our laboratory to test different models, approaches, and algorithms of spectrum simulation. Thus, it is not a finished software product, and it is not optimized by efficiency. Nevertheless, we believe that the program can be useful to reproduce the presented results or treat similar spectral data.

The program is written using Fortran, but as different subprograms were created by different programmers, in different times, and with different aims, the project as a whole does not meet any language standard. Of course, this circumstance produces troubles at compilation and debugging of the program. The program is presented free for any use with the only conditions that the authors are not responsible for any consequences and insist on citation of the source if the results obtained using the program are published.

The program can be loaded from the site
<http://www.chem.msu.ru/eng/lab/chemkin/ODF3/>

The program allows taking into account the following:

1. Tilt of hfi-tensors relative to g-axes.
2. Forbidden transitions.
3. Convolution of the Gaussian and Lorentzian functions for description of the shape of individual spectral line (Voigt profile).
4. Anisotropy of the line widths described by the second-rank tensors of the Gaussian and Lorentzian line widths.
5. Tilt of the Gaussian and Lorentzian tensors relative to the g-axes.
6. Stochastic rotational oscillations of paramagnetic molecules with limited amplitude and high frequency (quasi-librations).
7. Tilt of the libration axes relative to the g-axes.
8. The orientation distribution functions of the paramagnetic probe.
9. Up to 5 magnetic nuclei.
10. Up to 5 different paramagnetic centers.

The EPR spectra are computed in accordance with explicit formulas presented in [81]. Two types of spectrum calculation can be performed. Both types of calculation use the Hamiltonian within the perturbation theory of the second order. The first type of calculation assumes the coincidence of g-tensor frame with hfi-tensor frame. The second type of calculation takes into account any tilt of hfi-tensors relative to g-axes and forbidden transitions.

The formats for the input-output files are described in the document ODF3.pdf that can be loaded from the same site with the examples of the program applications.

Program esrD

The purpose of the program esrD is the treatment of experimental EPR spectra and preparation of spectra to the fitting procedure. This preparation ordinarily involves removal of the unnecessary tails, subtraction of the base line or base spectrum, double integration, normalizing of area under the spectrum, etc. All these procedures can be carried out using the standard software. On the other hand, when the spectra were recorded in different and possibly irregular points of the magnetic field, the mentioned operations were rather time-consuming. The program esrD allows carrying out necessary operations with the set of such spectra at once. It is useful as well for visual comparison of experimental and calculated spectra.

The program is presented free for any use with only the conditions that the authors are not responsible for any consequences and insist on the citation of the source if the results obtained using the program are published. The program can be loaded from the site <http://www.chem.msu.ru/rus/lab/chemkin/esrD/>.

6. References

- [1] Buchachenko A.L, Wasserman A.M (1973) Stable Radicals, Moscow: Khimiya. 410 p. (in Russian).

- [2] Robinson B.H, Tomann H, Beth A.H, Fajer P, Dalton L.R (1985) In EPR and Advanced EPR Studies of Biological Systems. Dalton L.R, editor. Boca Raton: C.R.C.Press, pp. 68-72.
- [3] Kuznetsov A.N (1976) Spin Probe Method. Theory and Application. Moscow: Nauka. 210 p. (in Russian).
- [4] Schneider D, Freed J (1989) Calculation of slow motion magnetic resonance spectra: a user's guide in: Biological magnetic resonance. In: Berliner L.J, Reuben J, editors. Spin Labeling: Theory and Application. New York: Plenum Press. pp. 1-76.
- [5] Budil D.E, Lee S, Saxena S, Freed J.H (1996) Nonlinear-Least-Squares Analysis of Slow-Motion EPR Spectra in One and Two Dimensions Using a Modified Levenberg-Marquardt Algorithm. *J. Magn. Reson. A* 120: 155-189.
- [6] Xu D, Budil D.E, Ober C.K, Freed J.H (1996) Rotational diffusion and order parameters of a liquid crystalline polymer studied by ESR: molecular weight dependence. *J. Phys. Chem.* 100 (39): 15867-15872.
- [7] Polimeno A, Freed J (1995) Slow motional ESR in complex fluids: the slowly relaxing local structure model of solvent cage effects. *J. Phys. Chem.* 99: 10995-11006.
- [8] Earle K.A, Moscicki J.K, Polimeno A, Freed J (1997) A 250 GHz ESR study of o-terphenyl: dynamic cage effects above T_c. *J. Chem. Phys.* 106 (24): 9996-10015.
- [9] Barnes J.P, Freed J.H (1998) Dynamics and Ordering in Mixed Model Membranes of Dimyristoylphosphatidylcholine and Dimyristoylphosphatidylserine: A 250-GHz Electron Spin Resonance Study Using Cholestane. *Biophysical Journal* 75: 2532-2546.
- [10] Lou Y, Ge M, Freed J.H (2001) A multifrequency ESR study of the complex dynamics of membranes. *J. Phys. Chem. B* 105 (45): 11053-11056.
- [11] Dzikovski B, Tipikin D, Livshits V, Earle K, Freed J (2009) Multifrequency ESR study of spin-labeled molecules in inclusion compounds with cyclodextrins. *Phys. Chem. Chem. Phys.* 11: 6676-6688.
- [12] Nayeem A, Rananavare S.B, Sastry V.S.S, Freed J.H (1989) Heisenberg spin exchange and molecular diffusion in liquid crystals. *J. Chem. Phys.* 91: 6887-6905.
- [13] Salikhov K.M (2010) Contributions of Exchange and Dipole-Dipole Interactions to the Shape of EPR Spectra of Free Radicals in Diluted Solutions. *Appl. Magn. Reson.* 38: 237-256.
- [14] Freed J.H (1966) On Heisenberg Spin Exchange in Liquids. *J.Chem.Phys.* 45: 3452
- [15] Freed J.H (1967) Theory of saturation and double resonance effects in electron spin resonance spectra. II. Exchange vs. dipolar mechanisms. *J.Phys Chem.* 71: 38-51.
- [16] D.Marsh (1989) Experimental methods in spin-label spectral analysis In: Berliner L.J, Reuben J, editors. Spin Labeling: Theory and Application. New York: Plenum Press. pp. 255-304.
- [17] Chumakova N.A, Pergushov V.I, Vorobiev A.Kh, Kokorin A.I (2010) Rotational and Translational Mobility of Nitroxide Spin Probes in Ionic Liquids and Molecular Solvents. *Appl. Magn. Res.* 39: 409-421.

- [18] Molin Yu.N, Salikov K.M, Zamaraev K.I (1980) Spin Exchange. Principles and Applications in Chemistry and Biology. Berlin; New York: Springer-Verlag, 1980. 242 p.
- [19] Kokorin A.I in Method of Spin Labels and Probes: Problems and Perspectives (Nauka, Moscow, 1986) pp. 61-78
- [20] Kurban M.R, Peric M, Bales B.L (2008) Nitroxide spin exchange due to re-encounter collisions in a series of n-alkanes. *J. Chem. Phys.* 129: 064501.
- [21] Kurban M.R (2009) Experimental correlation of nitroxide recollision spin exchange with free volume and compressibility in alkane and aromatic compounds. *J. Chem. Phys.* 130: 104502.
- [22] Kurban M.R (2011) A study of the relation between translational and rotational diffusion through measurement of molecular recollision. *J. Chem. Phys.* 134: 034503.
- [23] Chumakova N.A, Nikitina V.A, Pergushov V.I (2012) *Russ.J.Phys.Chem.* In press.
- [24] Khairy K, Budil D, Fajer P (2006) Nonlinear-least-squares analysis of slow motional regime EPR spectra. *J. Magn. Reson.* 183: 152–159.
- [25] Dennis J.E, Gay D.M, Welseh R.E (1981) An Adaptive Nonlinear Least-Squares Algorithm. *ACM Transactions on Mathematical Software* 7(3): 348-383.
- [26] Abragam A, Bleaney B. (1970) Electron paramagnetic resonance of transition ions. Oxford: Clarendon press. 911 p.
- [27] Abramowitz M, Stegun I.A Eds. (1964) Handbook of Mathematical Functions. National Bureau of Standards 1050 p.
- [28] Lebedev Ya.S, Grinberg O.Ya, Dubinsky A.A, Poluektov O.G (1992) Investigation of Spin Labels and Probes by Millimeter Band EPR. In: Zhdanov R.I, editor. Bioactive Spin Labels. Berlin, Heidelberg, New York, London, Paris, Tokyo, Hong Kong, Barcelona, Budapest: Springer-Verlag.
- [29] Seber G.A.F, Wild C.J (1989) Nonlinear regression. New York: Wiley. 768 p.
- [30] Freed J.H (1976) Theory of slow tumbling ESR spectra for nitroxides. In: Berliner L.J, editor. Spin Labeling: Theory and applications. New York: Academic Press. pp. 53-132.
- [31] Chernova D.A, Vorobiev A.Kh (2009) Temperature Dependence of ESR Spectra of Nitroxide Spin Probe in Glassy Polymers. *Journal of Polymer Science: Part B: Polymer Physics.* 47: 563–575.
- [32] Redfield A.G (1966) The theory of relaxation processes. *Adv. Magn. Res.* 1: 1–32.
- [33] Kuznetsov A.N, Wasserman A.M, Volkov A.U, Korst N.N (1971) Determination of rotational correlation time of nitric oxide radicals in a viscous medium. *Chem.Phys.Lett.* 12(1): 103-105.
- [34] Kovarski A.L (1997) Molecular dynamics of Additives in Polymers. Utrecht: VSP. 276 p.
- [35] Polanszek C.F, Freed J.H (1975) Electron spin resonance studies of anisotropic ordering, spin relaxation, and slow tumbling in liquid crystalline solvents. *J Phys Chem.* 79: 2283–2306.
- [36] Meirovitch E, Nayaman A, Freed J.H (1984) Analysis of protein-lipid interactions based on model simulations of electron spin resonance spectra. *J Phys Chem.* 88: 3454–3465.

- [37] Meirovitch E, Freed J.H (1984) Analysis of slow-motional electron spin resonance spectra in smectic phases in terms of molecular configuration, intermolecular interactions, and dynamics. *J Phys Chem.* 88: 4995–5004.
- [38] Chernova D.A, Vorobiev A.K (2011) Molecular Mobility of Nitroxide Spin Probes in Glassy Polymers: Models of the Complex Motion of Spin Probes. *Journal of Applied Polymer Science.*121(1): 102–110.
- [39] Bercu V, Martinelli M, Massa C.A, Pardi L.A, Rossler E.A, Leporini D. (2008) Anomaly of the rotational nonergodicity parameter of glass formers probed by high field electron paramagnetic resonance. *J Chem Phys.*129: 081102.
- [40] Maresch G.G, Weber M, Dubinskii A.A, Spiess H.W (1992) 2D-ELDOR detection of magnetization transfer of nitroxides in disordered solid polymers. *Chem Phys Lett.* 193: 134-140.
- [41] Dzuba S.A, Tsvetkov Y.D, Maryasov A.G. (1992) Echo-induced EPR spectra of nitroxides in organic glasses: model of orientational molecular motions near equilibrium position. *Chem Phys Lett.* 188: 217-222.
- [42] Dzuba S.A. (1992) Echo-induced EPR spectra of nitroxides: Study of molecular librations. *Pure Appl Chem.* 64(6): 825-831.
- [43] Dzuba S.A (1996) Libration motion of guest spin probe molecules in glassy media. *Phys Lett A.* 213(1-2): 77-84.
- [44] Dzuba S.A (2000) Libration motion of guest spin probe molecules in organic glasses: CW EPR and electron spin echo study. *Spectrochim Acta A.* 56(2): 227-234.
- [45] Van S. P, Birrell G. B, Griffith O. H (1974) Rapid anisotropic motion of spin labels. Models for motion averaging of the ESR parameters. *J Magn Reson.* 15: 444–459.
- [46] Griffith O, Jost P. (1976) Instrumental aspects of spin labeling. In: *Spin Labeling, Theory and Applications.* Berliner L.J, editor. New York: Academic Press. pp 251–272.
- [47] Chernova D.A, Vorobiev A.Kh (2009) Molecular Mobility of Nitroxide Spin Probes in Glassy Polymers. Quasi-Libration Model. *Journal of Polymer Science: Part B: Polymer Physics.* 47: 107–120.
- [48] Vorobiev A.K, Gurman V.S, Klimenko T.A (2000) Rotational mobility of guest molecules studied by method of oriented spin probe. *Phys Chem Chem Phys.* 2(3): 379–385.
- [49] Vorob'ev A.K, Gurman V.S, Klimenko T.A (2000) Models of slow rotational mobility of paramagnetic probes in glassy media. *Russ Chem Bull.* 49: 1059–1067.
- [50] Paschenko S.V, Toropov Y.V, Dzuba S.A, Tsvetkov Y.D, Vorobiev A.K (1999) Temperature dependence of amplitudes of libration motion of guest spin-probe molecules in organic glasses. *J Chem Phys.* 110: 8150–8154.
- [51] Tenhu H, Rantala J, Samarinov B, Timofeev V (1998) Phase transitions of poly(octyl isocyanate). *Polymer.* 39: 4057–4063.
- [52] Timofeev V, Samarinov B (1995) Dynamics of macromolecule spin-labelled side-chain groups by electron paramagnetic resonance spectra simulation. *J Chem Soc Perkin Trans. 2:* 2175–2181.

- [53] Vekšli Z, Andreis M, Rakvin B (2000) ESR spectroscopy for the study of polymer heterogeneity. *Prog. Polymer Sci.* 25(7): 949-986.
- [54] Dzuba S.A, Salnikov E.S., Kulik L.V (2006) CW EPR, echo-detected EPR, and fieldstep ELDOR study of molecular motions of nitroxides in o-terphenyl glass: Dynamical transition, dynamical heterogeneity and beta-relaxation. *Appl. Magn. Reson.* 30(3-4): 216-222.
- [55] Cameron G.G, Miles I.S, Bullock A.T (1987) Distribution in correlation times for rotational diffusion of spin probes in polymers. *Br. Polymer J.* 19: 129-134.
- [56] Faetti M, Giordano M, Leporini D, Pardi L (1999) Scaling analysis and distribution of the rotational correlation times of a tracer in rubbery and glassy poly(vinyl acetate). *Macromolecules.* 32(6): 1876 -1882.
- [57] Shantarovich V.P, Kevdina I.B, Yampolskii Y.P, Alentiev A.U (2000) Positron Annihilation Lifetime Study of High and Low Free Volume Glassy Polymers: Effects of Free Volume Sizes on the Permeability and Permselectivity. *Macromolecules.* 33: 7453–7466.
- [58] Bercu V, Martinelli M, Massa C.A, Pardi L.A, Leporini D (2005) Signatures of the fast dynamics in glassy polystyrene: First evidence by high-field Electron Paramagnetic Resonance of molecular guests. *J Chem Phys.* 123: 174906.
- [59] Saalmueller J.W, Long H.W, Maresch G.G, Spiess H.W (1995) Two-Dimensional Field-Step ELDOR. A Method for Characterizing the Motion of Spin Probes and Spin Labels in Glassy Solids. *J Magn Reson A.* 117(2): 193-208.
- [60] Saalmueller J.W, Long H.W, Volkmer T, Wiesner U, Maresch G.G, Spiess H.W (1996) Characterization of the motion of spin probes and labels in amorphous polymers with two-dimensional field-step ELDOR. *J Polym Sci Part B Polym Phys.* 34(6): 1093-1104.
- [61] Bogdanov A.V, Vorobiev A.Kh (2011) Rotational mobility and rate of photoisomerization of spin-labeled azobenzenes in glassy polystyrene. *Chemical Physics Letters* 506: 46–51.
- [62] Nakatsuji S, Fujino M, Hasegawa S, Akutsu H, Yamada J, Gurman V.S, Vorobiev A.Kh (2007) Azobenzene Derivatives Carrying A Nitroxide Radical. *J.Org.Chem.* 72: 2021-2029.
- [63] Friesner R., Nairn J.A, Sauer K (1979) Direct calculation of the orientational distribution function of partially ordered ensembles from the EPR line shape. *J. Chem. Phys.* 71(1): 358-365.
- [64] Friesner R., Nairn J.A (1980) A general theory of the spectroscopic properties of partially ordered ensembles. I. One vector problems *J. Chem. Phys.* 72 (1): 221-230.
- [65] Shimada S., Hori Y., Kashiwabara H (1985) Structure of Peroxy Radicals Trapped in Irradiated Isotactic Polypropylene and Molecular Disorder of the Polymer Chain, Related with Hydrogen Abstraction Reaction of the Radicals. *Macromol.* 18: 170-176.
- [66] Shimada S., Hori Y., Kashiwabara H (1988) Distribution of Molecular Orientation and Stability of Peroxy Radicals in the Noncrystalline Region of Elongated Polypropylene. *Macromol.* 21: 979-982.

- [67] Swartz J.C, Hoffman B.M, Krizek R.J, Atmatzidis D.K (1979) A General Procedure for Simulating EPR Spectra of Partially Oriented Paramagnetic Centers. *J. Magn. Res.* 36: 259-268.
- [68] Hentschel R, Schilitter J, Sillescu H, Spiess H.W (1978) Orientational distributions in partially ordered solids as determined from NMR and ESR line shapes. *J. Chem. Phys.* 68: 56-66.
- [69] Ovchinnikov I.V, Konstantinov V.N (1990) EPR line shape of orientationally ordered solid systems. In: Zaripov M.M, editor. *Radio-spectroscopy of the condensed media.* Moscow: Nauka. pp. 90-110 (in Russian)
- [70] Ajtai K, French A.R, Burghardt Th.P (1989) Myosin cross-bridge orientation in rigor and in the presence of nucleotide studied by electron spin resonance. *Biophys. J.* 56: 535-541.
- [71] Burghardt Th.P, Thompson N.L (1985) Model-independent electron spin resonance for measuring order of immobile components in a biological assembly. *Biophys. J.* 48: 401-409.
- [72] Caldeira J, Figueirinhas J.L, Santos C, Godinho M.H (2004) EPR spectroscopy of protein microcrystals oriented in a liquid crystalline polymer medium. *J. Magn. Reson.* 170: 213-219.
- [73] Vorobiev A.Kh, Chumakova N.A (2005) Determination of orientation distribution function of anisotropic paramagnetic species by analysis of ESR spectra angular dependence. *J. Magn. Reson.* 175: 146-157.
- [74] Vorob'ev A.Kh, Chumakova N.A (2005) Determination of molecular orientation distribution of a stable paramagnetic probe in oriented 4-cyano-4'-n-pentylbiphenyl. *Russ.Chem.Bull.* 54(1): 195-200
- [75] Chumakova N.A, Vorobiev A.Kh, Ikuma N, Uchida Y, Tamura R (2008) Magnetic characteristics and orientation of a new nitroxide radical in an ordered matrix, *Mendeleev. Commun.* 18: 21-23.
- [76] Chumakova N.A, Pomogailo D.A, Yankova T.S, Vorobiev A.Kh (2011) The novel stable nitroxide radicals as perspective spin probes for study of orientation order of liquid crystals and polymers. *Mol. Cryst. Liq. Cryst.* 540: 196-204.
- [77] Yankova T.S, Chumakova N.A, Vorobiev A.Kh (2008) Orientation distribution function of HO₂· radicals ordered by light irradiation. *Appl. Magn. Res.* 33: 117-126.
- [78] Elyashevich G, Kozlov A, Moneva I (1998) Study of polyethylene orientation in the course of porous structure formation. *J. Polym. Sci. series B.* 40: 71-74 [*Vysokomol. Soyed.* 40: 483-486, in Russian].
- [79] Michl J, Thulstrup E.W (1986) *Spectroscopy with polarized light: Solute Alignment by Photoselection, in Liquid Crystals, Polymers and Membranes.* New York: VCH Publishers. 573 p.
- [80] Yankova T.S, Chumakova N.A, Vorob'ev A.Kh (2011) Photoinduced Orientational Order of Dichloride Anion Radicals, *Russian Journal of Physical Chemistry A* 85 (4): 695-701.

- [81] Zhidomirov G.M., Lebedev Ia.S., Dobriakov C.A., Shtenshneider N.Ia., Chirkov, A.K., Gubanov V.A. (1975) Interpretation of complex EPR spectra, Moscow: Nauka, , 216 p. (in Russian).

IntechOpen

IntechOpen